Non-linear power spectra of dark and luminous matter in halo model of structure formation

Yurij Kulinich,* Bohdan Novosyadlyj,† and Stepan Apunevych‡
Astronomical Observatory of Ivan Franko National University of Lviv, Kyryla i Methodia str., 8, Lviv, 79005, Ukraine
(Dated: March 1, 2013)

The paper represents a comprehensive treatment of late stages of large-scale structure evolution within the framework of halo model. A number of modifications to basic theory are suggested. We have engineered simple yet accurate approximation to relate the amplitude of non-linear spherical density perturbation to the one of the linear. The theory for final stages of spherical overdensity evolution is revised in order to re-evaluate the dependences of collapse and critical overdensity parameters, δ_{col}, δ_{ta} and δ_{min}, on redshift and other cosmological parameters. A new technique is proposed for straightforward computation of halo concentration parameter, c, without need to evaluate the z_{col}. Validity of the technique is proved for a number of ΛCDM and ΛWDM cosmologies. The parameters for Sheth-Tormen mass function are estimated, as well as new approximation is constructed for the dependence of subhalo mass function on initial power spectrum. The modified and extended halo model is applied to the determination the non-linear dark matter and galaxy power spectra. The semi-analytical estimation of dark matter power spectrum is verified by comparison with data from numerical simulations. Also the predictions for the galaxy power spectra are confronted with 'observed' data from PSCz and SDSS galaxy catalogs. Quite good accordance is found.

PACS numbers: 95.36.+x, 98.80.-k
Keywords: cosmology: large scale structure of Universe – non-linear evolution – power spectra

I. INTRODUCTION

A commonly accepted inflationary paradigm states that the large-scale structure (LSS) of the Universe is formed through evolution of density perturbations driven by gravitational instability. Seeded by quantum fluctuations, the perturbations are initially small in amplitude, they are expanded by inflation afterwards and develop during different epochs when medium is dominated by density of radiation, matter and dark energy consequently. A number of manifestations of large-scale structure are available for observation: spatial distribution of the luminous objects (galaxies, clusters), cosmic microwave background (CMB) anisotropy, the features in the spectra of high-redshift quasars (Ly_α-clouds), as well as the probes via gravitational lensing. The statistics, e.g. correlations functions or power spectra, can be drawn from observational data to test cosmological models and scenarios of large-scale structure formation.

At some point of evolution the growth of perturbations of small scales switches to non-linear regime. The linear power spectrum is well-understood, for $k < 0.1$ hMpc^{-1} the transfer functions can be readily computed at percent accuracy for any feasible cosmology. It is not so for the small-scale non-linear power spectrum, mostly due to the non-linear terms in equations, along with complex physics of processes taking place in baryonic component (hydrodynamics, radiation transfer, thermal and chemical evolution). At final stages the dynamical relaxation leads to galaxy formation. The aim of this paper is to develop a technique, capable to build a bridge between the initial matter power spectrum and observable galaxy power spectra inherently non-linear at small scales. The treatment is based on the halo model complemented by analytical approximations, the results are tested and verified against data of N-body simulations.

The N-body simulation is a most powerful tool that is used to study the structure formation, especially at non-linear scales. The numerical simulation technique requires input data, usually this is initial distribution of the matter particles, to be generated by some special procedure [1, 2] for given primordial matter power spectrum. Also the cosmology should be defined, namely the nature of dark components, values of cosmological parameters, etc.

Within standard scenario introduced in [3], the gravitational potential of collisionless dark matter shapes the wells to which the previously oscillating baryonic matter falls in after the decoupling, until the baryonic matter power spectrum reaches the amplitude of dark matter power spectrum. At some point, a non-linear perturbation with amplitude exceeding some critical detaches from background expansion, reaches a turnaround point, and the collapse starts due to self-gravity. The processes of violent relaxation take place subsequently, and the virial equilibrium has been set in result, the halo of dark matter is formed. The baryonic gas starts to gradually cool, fragments into clouds and the luminous tracers inside halos are ignited (see [4, 5] for details).

Thus, the spatial distribution of luminous matter

*Electronic address: kul@astro.franko.lviv.ua
†Electronic address: novos@astro.franko.lviv.ua
‡Electronic address: apus@astro.franko.lviv.ua

should strongly correlate with halo one. The correlation is inferred from large simulations which take into complete account the baryon physics and particle dynamics of dark matter [6, 7], as well as from semi-analytic models of galaxy formation [8–10]. The numerical technique requires the considerable computing power, whereas the purely analytical is found unreliable. Thus, the "hybrid" approach seems to be optimal, combining the analytical model of galaxy formation [11, 12] with dark matter "merger trees" extracted from simulations, meanwhile the gas dynamics is treated empirically. However, we are still far from full understanding of the physics of various processes governing the galaxy formation, we can not still yield predictions accurate enough. Therefore, the alternative way is to extract the halo and subhalo statistics from simulations, to build the appropriate approximations and compare the results with observables from large galaxy surveys, such as luminosity, color, morphology, stellar masses etc. The descriptions used in such techniques include the conditional luminosity function (CLF) [13–15], conditional mass function (CMF) [16] and stellar mass to halo mass relation [16, 17].

The halo model is a cornerstone of modern theory of structure formation. It has been proven to be well-motivated, comprehensive and provides plausible explanation for observational data and results of cosmological simulations. It is valid for wide range of cosmologies, as long as the statistics of primordial density perturbations is Gaussian. It encompasses the non-linear stage of evolution of density perturbations as well as the dynamical relaxation processes assuming that all mass is associated with gravitationally bound virialized halo.

It was shown in papers [18–20] that given the halo statistics, known internal structure of halo and spatial distribution of halos, it is possible to evaluate the non-linear power spectrum of dark matter perturbations. At the next step, the initial power spectrum can be reconstructed by applying the halo model to the data of N-body simulations. For example, the halo occupation function, $p(N|M)$, was used in [21] to describe the probability of finding N galaxies within a halo of mass M, to complement the halo model and to enable thus the calculation the non-linear galaxy power spectrum. However, regardless of overall success of the halo model[1] in giving the description of dark matter and galaxy clustering, it is still not complete. For instance, only the latest enhancements proposed in [23, 24] take into account the halo morphology and internal structure.

The halo model theory is based on the consideration of some individual spherical inhomogeneity evolving from early initial state to some point of turnaround, moment of collapse and formation of virialized halo. The information about such evolution is compressed into few generic parameters, namely the amplitude of linear density perturbation at turnaround point, δ_{ta}, the same amplitude at the moment of collapse of central homogeneous core of perturbation, δ_{col}, and the relative density of virialized halo, Δ_{vc} (in the literature often is denoted byΔ_c). All these parameters depend on the cosmology, primarily on the curvature of 3-space and content of dark energy.

In section 2 we analyze the evolution of a spherical perturbation in different cosmologies, in order to build analytical approximations applied henceforth in halo model. Also, the new technique is proposed there for computation of concentration parameter c for halo with Navarro-Frenk-White density profile.

The section 3 is devoted to the analysis of dark matter and galaxy clustering, by means of the halo model modified by including statistics drawn from simulations. In section 4 the model is applied to estimation of the initial power spectrum of dark matter from 'observable' galaxy power spectra, which are derived in [25, 26] from PSCz and SDSS galaxy catalogs respectively. The dependence of subhalo mass function (see [27]) on initial power spectrum is investigated, the new approximations are proposed for it. The non-linear stage of evolution is discussed therein. The conclusions are presented in section 5. All computations were performed for ΛCDM (cold dark matter with Λ-term) and ΛWDM (warm dark matter with Λ-term) cosmological models, some bulk mathematical derivations are moved into appendices.

II. FORMATION OF INDIVIDUAL SPHERICAL HALO

A. Background cosmological model

We assume that Universe is a homogeneous and isotropic space-time with line-element in the general form

$$ds^2 = dt^2 - a^2(t)\mathcal{M}^2(R)dR^2 - a^2(t)\chi^2(R)(d\theta^2 + \sin^2\theta d\varphi^2), \tag{1}$$

where t is cosmological time and R, θ, φ are spherical coordinates of 3-space with curvature K ($c = 1$ here and henceforth). The functions $\chi(R)$ and $\mathcal{M}(R)$ are related by

$$\frac{d\chi(R)}{dR} = (1 - K\chi^2(R))^{1/2}\mathcal{M}(R).$$

Either $\chi(R)$ or $\mathcal{M}(R)$ can be defined deliberately because an arbitrary transformation of the kind $R \to \tilde{R}(R)$ is allowed. For example, setting $\mathcal{M}(R) = 1$ leads to the commonly used line-element with

$$\chi(R) = \begin{cases} R & \text{for } K = 0; \\ \sin(\sqrt{K}R)/\sqrt{K} & \text{for } K > 0; \\ \sinh(\sqrt{|K|}R)/\sqrt{|K|} & \text{for } K < 0 \end{cases} \tag{2}$$

Assuming $\chi(R) = R$ we obtain other well-known form with $\mathcal{M}(R) = (1 - KR^2)^{-1/2}$.

[1] The details of halo model can be found in [22].

Another assumption is that expansion of the Universe is described by the Einstein's equations with cosmological constant,

$$\mathcal{G}_{\mu\nu} \equiv \mathcal{R}_{\mu\nu} - \frac{1}{2} g_{\mu\nu}\mathcal{R} = 8\pi G T_{\mu\nu} + g_{\mu\nu}\Lambda, \qquad (3)$$

where $\mathcal{R}_{\mu\nu}$ is Ricci tensor in the space-time with metric $g_{\mu\nu}$ defined by (1) and $T_{\mu\nu}$ is an energy-momentum tensor of matter. After recombination epoch the energy-momentum tensor is the one of pressureless ideal fluid with energy density $\overline{\rho}_m(t)$, $T^{\mu}_{\nu} = diag\{\overline{\rho}_m(t), 0, 0, 0\}$, expressed in comoving reference system. The matter includes the baryons and dark matter, which assumed to be of the cold or warm type. The dimensionless quantities of matter density, curvature and cosmological constant are defined as

$$\Omega_m \equiv \frac{8\pi G\rho^0_m}{3H_0^2}, \qquad \Omega_\Lambda \equiv \frac{\Lambda}{3H_0^2}, \qquad \Omega_K \equiv \frac{-K}{H_0^2}, \quad (4)$$

(ρ^0_m is mean density of dust matter and H_0 is Hubble parameter at present moment of time). The Einstein's equations (3) along with the differential energy-momentum conservation law lead to the Friedmann equations in the commonly used form

$$H = H_0 \left(\Omega_m/a^3 + \Omega_K/a^2 + \Omega_\Lambda\right)^{\frac{1}{2}}, \qquad (5)$$

$$q = \frac{H_0^2}{H^2}\left(\frac{1}{2}\Omega_m/a^3 - \Omega_\Lambda\right), \qquad (6)$$

with $H \equiv \dot{a}/a$ as Hubble parameter and $q \equiv -a\ddot{a}/\dot{a}^2$ as deceleration parameter at any moment of time (overdot denotes d/dt). For current epoch $t = t_0$, the equations are simple: $\Omega_m + \Omega_K + \Omega_\Lambda = 1$ and $q_0 = \Omega_m/2 - \Omega_\Lambda$.

B. Spherically symmetrical perturbation

Now let us analyze the non-linear stage of evolution of perturbation with spherical symmetry in different cosmologies in order to determine the dependences of the characteristic amplitudes on curvature, cosmological constant and matter density. Within Tolman's approach [28] the Einstein's equations (3) have analytical solutions for spherically symmetrical inhomogeneity in the synchronous gauge (*i.e.* in the frame comoving to the dust-like matter component). The space-time interval in this case has the form

$$ds^2 = dt^2 - e^{\lambda(t,R)}dR^2 - r^2(t,R)\left(d\theta^2 + \sin^2\theta d\varphi^2\right), \quad (7)$$

where t is proper time of observers at any R. Henceforth it is designated by τ after rescaling to units of H_0^{-1}.

For the metric (7) the Einstein equation $\mathcal{G}^0_1 = 0$ yields

$$\frac{\partial}{\partial\tau} r'^2 e^{-\lambda} = 0$$

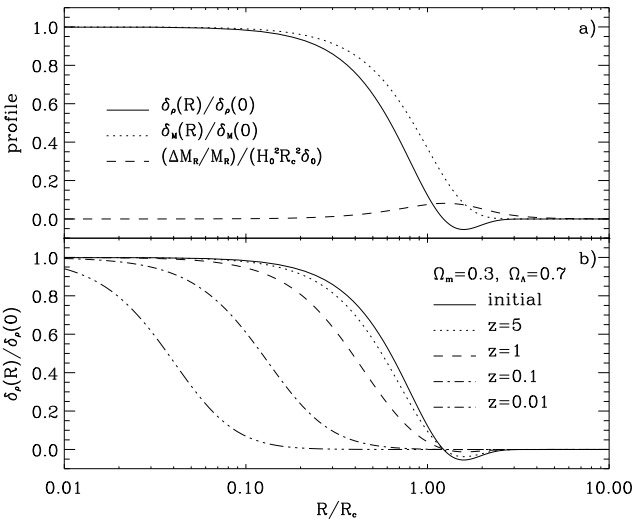

FIG. 1: Top panel: The initial profiles of spherical perturbation of density, $\delta_\rho(R)$, and mass, $\delta_M(R)$, both renormalized to their central values. The relative gravitational mass defect, $\Delta M_R/M_R$, is presented in the units of relative mass defect for homogeneous perturbations with the equivalent local curvature $\Omega_f(R)$: $H_0^2R^2\Omega_f(R)$. Bottom panel: The evolution of density profile at linear and weakly non-linear stages, as well as for non-linear stage (collapse). The value of initial amplitude is tuned in a specific way to provide turnaround point at $z = 2.5$ and complete collapse of central core at $z = 0$ in cosmology with $\Omega_m = 0.3$ and $\Omega_\Lambda = 0.7$.

(here and below $(') \equiv d/dR$). Because the product $r'^2e^{-\lambda}$ is a function of solely comoving radial coordinate R, the last equation is rewritten as

$$r'^2 e^{-\lambda} = 1 - f(R), \qquad (8)$$

where function $f(R)$ is relevant to initial conditions for perturbation, its density amplitude and profile at some early moment of time, as it will be shown below.

At some early epoch the amplitudes of metric perturbations are quite small, so the metric (7) converges to (1). Consequently, in the limit $\tau \to 0$ the terms $r(\tau, R) \to a(\tau)\chi(R)$ and $e^{\lambda(\tau,R)/2} \to a(\tau)\mathcal{M}(R)$. As the spherical perturbation is local overdensity with some characteristic scale R_c at $R \gg R_c$ the terms $r(\tau, R) \approx a(\tau)\chi(R)$ and $e^{\lambda(\tau,R)/2} \approx a(\tau)\mathcal{M}(R)$.

Let us introduce two variables $x(\tau, R) \equiv r(\tau, R)/\chi(R)$ and $y(\tau, R) \equiv e^{\lambda(\tau,R)/2}/\mathcal{M}(R)$, which are ratios of corresponding components of metric (7) and (1). The dependence of matter density on time and space coordinates in the region of perturbation can be presented as

$$\rho(\tau, R) = \rho^0_m x^{-2}(\tau, R) y^{-1}(\tau, R),$$

that follows from the differential energy-momentum conservation law, $T^{\mu}_{0;\mu} = 0$. At early epoch, the amplitude of perturbation is small and the components of metric (7) can be presented as linear expansion around corresponding values of background metric (1). The intro-

duced variables $x(\tau, R)$ and $y(\tau, R)$ as well as relative density perturbation $\delta_\rho(\tau, R)$, defined as

$$\delta_\rho(\tau, R) \equiv \frac{\rho_m(\tau, R)}{\overline{\rho}_m(\tau)} - 1, \tag{9}$$

are represented by linear approximations at this epoch,

$$x(\tau, R) \simeq a(\tau)\left(1 - \frac{1}{3}a(\tau)\alpha(R)\right), \tag{10}$$

$$y(\tau, R) \simeq a(\tau)\left(1 - \frac{1}{3}a(\tau)\beta(R)\right), \tag{11}$$

$$\delta_\rho(\tau, R) \simeq a(\tau)A(R). \tag{12}$$

Here, the functions $\alpha(R)$ and $\beta(R)$ describe the radial dependence of spatial components of metric (7) and the function $A(R) \equiv (2\alpha(R) + \beta(R))/3$ is the initial profile of density perturbation [29, 30].

From Eq. (8) and expansions (10)-(11) two relations follow: $\chi'(R)\beta(R) = \chi'(R)\alpha(R) + \chi(R)\alpha'(R)$ and $\alpha(R) = 3\chi^{-3}(R)\int_0^R A(R)\chi^2(R)\chi'(R)dR$, by which the radial dependences of metrics components can be determined for given profile of initial density perturbation [29, 30]. The Einstein equation $\mathcal{G}_0^0 = 8\pi G\rho_m + \Lambda$ and approximations (10)-(12) yield the equality

$$\frac{40}{3}\pi G\rho_m^0 A(R)\chi^2(R)\chi'(R) = \frac{\partial}{\partial R}(f(R)\chi(R) - K\chi^3(R)). \tag{13}$$

With local curvature parameter defined as

$$\Omega_f(R) \equiv -f(R)/(H_0^2\chi^2) \tag{14}$$

by integration of Eq. (13) we arrive to the expression which relate the local curvature to the radial profile of initial density perturbation and curvature of background space,

$$\Omega_f(\chi) = -5\Omega_m\chi^{-3}\int_0^\chi A(\chi)\chi^2 d\chi + \Omega_K. \tag{15}$$

This expression along with definition (14) allows the function $f(R)$, introduced in (8), to be represented via profile of initial density perturbation.

Thus, the spherically symmetrical perturbation is completely defined by defining its initial profile A as function of χ. In case of $\chi(R) = R$ the expression (15) is like

$$\Omega_f(R) = -5\Omega_m R^{-3}\int_0^R A(\tilde{R})\tilde{R}^2 d\tilde{R} + \Omega_K. \tag{16}$$

The profile of initial density perturbation can be chosen deliberately, just for simplicity of derivations we put it in the form

$$A(\xi) = \delta_0\left(1 - \frac{2}{3}\xi^2\right)e^{-\xi^2}, \tag{17}$$

$\xi \equiv R/R_c$, where R_c is a characteristic scale and δ_0 is an amplitude of perturbation [31]. Given that, the Eq. (16) transforms into

$$\Omega_f(\xi) = -\frac{5}{3}\Omega_m\delta_0 e^{-\xi^2} + \Omega_K. \tag{18}$$

For $R \gg R_c$ it is readily seen, that the metric (7) converges to (1), as $\Omega_f(R)$ asymptotically approaches Ω_K.

The general equations for variables $x(\tau, R)$ and $y(\tau, R)$ are derived from Einstein's equations $\mathcal{G}_1^1 = \Lambda$ and $\mathcal{G}_2^2 - \frac{1}{2}\mathcal{G}_1^1 = \frac{1}{2}\Lambda$ as follows

$$\ddot{x} = \frac{3}{2}\Omega_\Lambda x - \frac{1}{2}\frac{\dot{x}^2}{x} + \frac{1}{x}\frac{\Omega_f}{2}, \tag{19}$$

$$\ddot{y} = \frac{3}{2}\Omega_\Lambda y - \left(\frac{\dot{x}\dot{y}}{x} - \frac{1}{2}\frac{\dot{x}^2 y}{x^2}\right) + \left(\Omega_f + R\frac{\Omega_f'}{2}\right)\frac{1}{x} - \frac{y}{x^2}\frac{\Omega_f}{2} \tag{20}$$

Here and henceforth a derivative with respect to τ is denoted by overdot. The initial conditions are adiabatic and refer to some early moment of time, $\tau_i = \frac{2}{3}{\Omega_m}^{-1/2}a_i^{3/2}$ $(a_i \ll 1)$: $x_i = a_i(1 - a_i\alpha(R)/3)$, $y_i = a_i(1 - a_i\beta(R)/3)$, $\dot{x}_i = \dot{a}_i(1 - 2a_i\alpha(R)/3)$, $\dot{y}_i = \dot{a}_i(1 - 2a_i\beta(R)/3)$ and $\Omega_f(R)$ is given by (15).

The first integral of (19) is $\dot{x}^2 - F(R)/(R^3H_0^2)x^{-1} - \Omega_\Lambda x^2 = \Omega_f$. Here $F(R) = 2GM_R$ (see [32]), the $M_R \equiv 4\pi\int_0^R \rho_m r^2 r' dR$ is the mass of matter contained within the sphere of radius R, and the curvature of space is not considered. Hence, we arrive to

$$\dot{x}^2 - \frac{\Omega_m}{x} - \Omega_\Lambda x^2 = \Omega_f. \tag{21}$$

The total (gravitational) mass within the sphere of radius R is $\tilde{M}_R \equiv 4\pi\int_0^R \rho_m r^2 e^{\lambda/2}dR = 4\pi\rho_m^0\int_0^R R^2(1 + H_0^2R^2\Omega_f(R))^{-1/2}dR$. The difference $\Delta M_R \equiv M_R - \tilde{M}_R$ is called a gravitational mass defect. It can be either negative or positive, depending on the sign of the local curvature, Ω_f. The relative mass perturbation $\delta_M \equiv \delta M_R/M_R$ in the sphere of radius R, see [32], is

$$\delta_M(\tau, R) = \frac{3}{r^3(\tau, R)}\int_0^R \delta_\rho(\tau, R)r^2(\tau, R)r'(\tau, R)dR = \frac{a^3(\tau)}{x^3(\tau, R)} - 1. \tag{22}$$

Thus, the value $\rho_M(\tau, R) \equiv \rho_m^0 x^{-3}(\tau, R)$ is a mean matter density in the sphere of radius R, and $\rho(\tau, R) \equiv \rho_m^0 x^{-2}(\tau, R)y^{-1}(\tau, R)$ is a matter density at radius R from the center of perturbation. The initial profile of density perturbation (17) and corresponding profile of mass perturbation $\delta_M(R)$ are shown in Fig. 1a, renormalized to the central values. The relative mass defect is presented in the units of relative mass defect of the homogeneous perturbations with the same value of local curvature $\Omega_f(R)$ at any R: $H_0^2R^2\Omega_f(R)$.

Within the approach we are developing here, the mass $M(R)$ keeps constant value for any R. It means that

equations (19) and (20) are valid if $\Omega_f \leq \Omega_K$ and $\Omega'_f \geq 0$ at any $R > 0$. In this case the first counter-flow of the dark matter component arises in the center of perturbation at moment of collapse[2], when $r(\tau_c, R < R_h) = 0$, the R_h is the radius of central homogeneous region (top). At this moment (τ_c) the equations (19)-(20) become singular for $0 < R < R_h$ and thus unusable.

The most of profiles of initial spherical overdensities relevant to cosmological applications can be described by the central amplitude and the characteristic radius (e.g. (17)). In the model with dust-like matter the growth of amplitude of central part does not depend on density distribution outside of it, and the time dependence of profile (and characteristic radius) is determined by the central amplitude. The evolution of density perturbation profiles is shown in Fig. 1b, with initial density profile given by (17) and value of central amplitude taken to provide turnaround point at $z = 2.5$ and finished collapse of central part at $z = 0$ in the cosmological model with $\Omega_m = 0.3$ and $\Omega_\Lambda = 0.7$.

The density and mass perturbations, as defined by (12) and (22) correspondingly, in the case of small amplitudes ($\ll 1$) can be approximated by

$$\delta_\rho(\tau, R) \simeq \delta(a(\tau), R) \equiv A(R) D\left(a(\tau)\right), \quad (23)$$

$$\delta_M(\tau, R) \simeq \overline{\delta}(a(\tau), R) \equiv \frac{3}{5}\frac{\Omega_K - \Omega_f(R)}{\Omega_m} D\left(a(\tau)\right) \quad (24)$$

Here, $D(a(\tau))$ is the growing mode of solution for density perturbation in the linear theory,

$$\ddot{\delta} + 2\frac{\dot{a}}{a}\dot{\delta} + \left(\frac{\ddot{a}}{a} - \frac{\dot{a}^2}{a^2} - \frac{K}{a^2}\right)\delta = 0. \quad (25)$$

It can be expressed in the integral form as follows

$$D(a) = \frac{5}{2}\Omega_m a^{-1} X^{1/2}(a) \int_0^a X^{-3/2}(\tilde{a}) d\tilde{a}, \quad (26)$$

where $X(a) \equiv \Omega_\Lambda a^2 + \Omega_m a^{-1} + \Omega_K$ [32, 33].

The evolution of a spherical inhomogeneity is accomplished in two stages: 1. The expansion stage ($\dot{x} > 0$, $\dot{\rho}_M < 0$), or linear and weakly non-linear regime; 2. The collapse stage ($\dot{x} < 0$, $\dot{\rho}_M > 0$), or fully non-linear regime. They are separated by the moment of turnaround, when $\dot{x} = 0$ ($\dot{\rho}_M = 0$).

The equations (21) and (20) can be integrated numerically for different cosmologies and values of δ_0 (an example of such computations is shown in Fig. 1). It is suitable to treat the evolution of non-linear perturbation by comparing it with the evolution of some fictional linear perturbation just extrapolated into non-linear stage.

[2] The final stages of collapse are not properly described by Eqs. (19)-(20) because the dust approximation fails at some high density, when the non-radial fluctuations take place and even the dark matter collisionless component undergoes the so-called violent relaxation before the virial equilibrium is set.

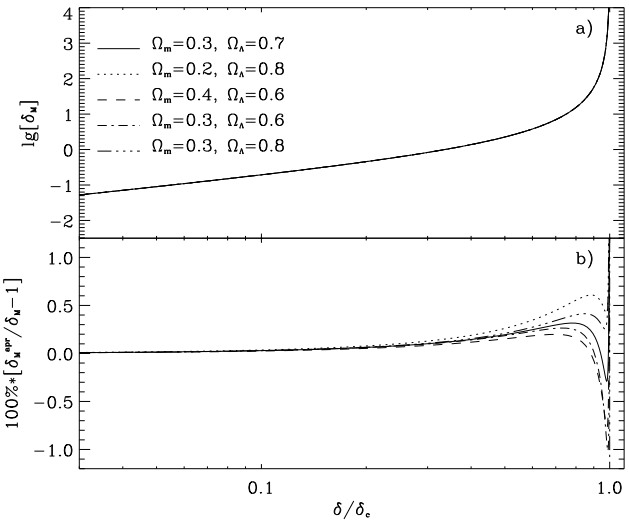

FIG. 2: The dependence of non-linear amplitude of spherical perturbation on the linear one (top panel). The accuracy of the approximation (27) for some cosmological models (bottom panel).

So, the time dependence of the perturbation amplitude is represented in terms of the ratio of amplitude of linear perturbation with initial mean overdensity $\overline{\delta}$ at some R to δ_{col}, the amplitude of perturbation which is to collapse at moment t_{col}. The dependence of non-linear amplitude calculated by integration of equations (21) and (20) upon the ratio $\overline{\delta}/\delta_{col}$ is shown in the top panel of Fig. 2 for some cosmological models.

The fit for the dependence is simple,

$$\begin{aligned} \lg\left[1 + \delta_M\right] \simeq & -\delta_{col} \cdot \lg\left[1 - \overline{\delta}/\delta_{col}\right] + A \cdot \lg^2\left[1 - \overline{\delta}/\delta_{col}\right] \\ & + B \cdot \lg^3\left[1 - \overline{\delta}/\delta_{col}\right], \end{aligned} \quad (27)$$

coefficients $A = 0.0903$ and $B = 0.0074$. The errors of the approximation lie within 1% range up to moment of finished collapse, when $\delta_M \to \infty$ (bottom panel of Fig. 2). The matter overdensity amplitude, δ_ρ, can be estimated from δ_M for any radius R by relation

$$\delta_\rho = \frac{1 + \delta_M}{1 + (\overline{\delta} - \delta)\frac{\partial}{\partial\delta}\ln(1 + \delta_M)} - 1. \quad (28)$$

C. The turnaround point and minimal amplitude

It was already mentioned, that the moment of turnaround is defined by equation $\dot{x} = 0$. The value of x at this moment, henceforth x_{ta}, is determined from the Eq. (21), which at this moment is simplified to

$$\Omega_\Lambda x_{ta}^3 + \Omega_f x_{ta} + \Omega_m = 0. \quad (29)$$

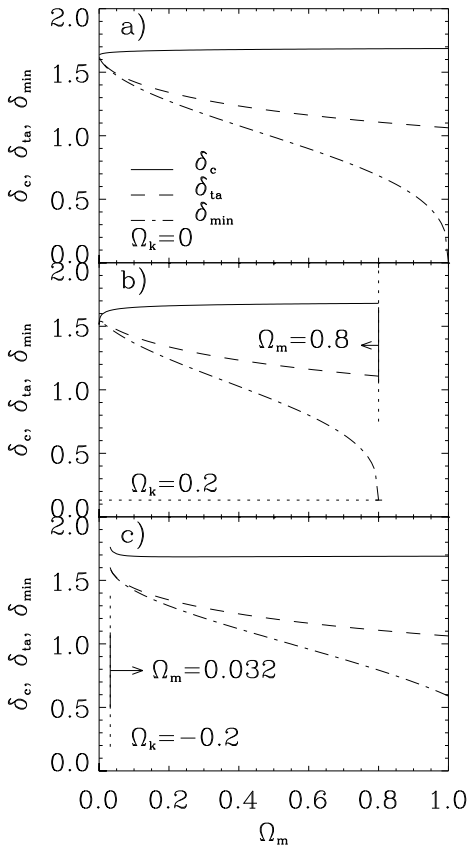

FIG. 3: The dependences of the critical amplitudes, δ_{col}, δ_{ta} and δ_{min}, on the matter content Ω_m, for different values of the curvature parameter: a) $\Omega_K = 0$, b) $\Omega_K = 0.2$, c) $\Omega_K = -0.2$.

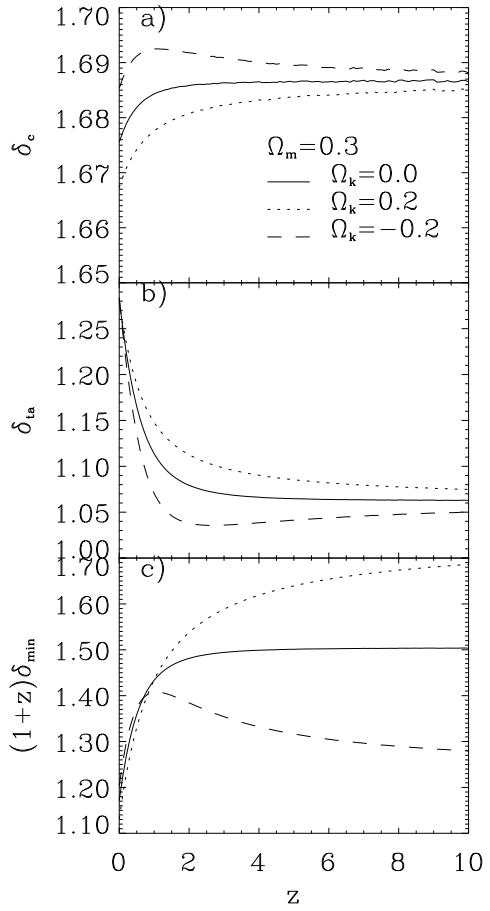

FIG. 4: Linear amplitudes of perturbation undergoing different stages at the time z: a) collapse, δ_{col}, b) turnaround, δ_{ta}, and c) asymptotic approach of turnaround, δ_{min}. The curvature takes the values $\Omega_K = 0, 0.2, -0.2$.

The solution for overdensity ($\Omega_f < 0$) in model with $\Omega_\Lambda > 0$ is

$$x_{ta} = \left(-\frac{4\Omega_f}{3\Omega_\Lambda}\right)^{\frac{1}{2}} \cos\left\{\frac{1}{3}\arccos\left[-\frac{\Omega_m}{2\Omega_\Lambda}\left(-\frac{3\Omega_\Lambda}{\Omega_f}\right)^{\frac{3}{2}}\right] - \frac{2\pi}{3}\right\} \qquad (30)$$

The moment of reaching turnaround point, τ_{ta}, can be evaluated by integration of Eq. (21):

$$\tau_{ta} = \int_0^{x_{ta}} \frac{dx}{(\Omega_m x^{-1} + \Omega_\Lambda x^2 + \Omega_f)^{1/2}}. \qquad (31)$$

The expression in denominator equals zero at $x = x_{ta}$, nevertheless the integral is finite.

In cosmology with $\Omega_\Lambda \leq 0$ or/and $\Omega_K \leq 0$, every perturbation which have positive amplitude ($\Omega_K - \Omega_f > 0$) can reach the turnaround point. However, in cosmology with $\Omega_\Lambda \geq 0$ or/and $\Omega_K \geq 0$, only perturbation with amplitude exceeding some critical value can do that. The condition of existence of turnaround point follows from Eq. (21): the perturbation stops the expansion at x_{ta} if function $\dot{x}^2(x)$ has extremum (minimum) at x_{ext} in which $\ddot{x}^2(x_{ext}) \leq 0$. The condition is $\Omega_f \leq -3(\Omega_m/2)^{2/3}\Omega_\Lambda^{1/3}$. The equality corresponds to the case of $x_{ta} = x_{ext}$ and $\dot{x} = \ddot{x} = 0$ (see Eq. (19)), therefore the point of expansion halt is geometrically a point of inflection not turnaround. This equation yields the minimal value of amplitude which a linear perturbation ought to acquire in order to arrive at the halt but never collapse completely

$$\delta_{min}(\tau) \equiv \frac{3}{5}\frac{\Omega_K + 3\,(\Omega_m/2)^{2/3}\,\Omega_\Lambda^{1/3}}{\Omega_m} D(a(\tau)). \qquad (32)$$

Only perturbations with linear amplitude $\delta(\tau) > \delta_{min}(\tau)$ can reach turnaround point followed by collapse and formation of virialized object for cosmologically justified time. In the Einstein-de Sitter cosmological model, $\Omega_m = 1$, $\Omega_\Lambda = \Omega_K = 0$, $\delta_{min} = 0$ and the value of δ_{ta} does not depend on the moment of turnaround and equals

$$\delta_{ta} = \frac{3}{5}\left[\frac{3\pi}{4}\right]^{2/3} \simeq 1.0624.$$

However, for the models with non-zero Λ-constant and/or curvature Ω_K, the value of δ_{ta} does depend on the mo-

ment of turnaround, $z_{ta} \equiv z(\tau_{ta})$. For instance, at given $z_{ta} > 5$, if the influence of Λ-constant is negligible ($\Omega_\Lambda \ll \Omega_m(1+z_{ta})^3$, $\Omega_\Lambda \ll \Omega_K(1+z_{ta})^2$) the proper linear amplitude of perturbation has simple asymptotic dependence on z_{ta}:

$$\delta_{ta}(z_{ta}) \simeq \frac{3}{5}\left[\frac{3\pi}{4}\right]^{\frac{2}{3}} + \frac{3}{5}\left(1 - \frac{13}{35}\left[\frac{3\pi}{4}\right]^{\frac{2}{3}}\right)\frac{\Omega_K}{\Omega_m(1+z_{ta})} \simeq 1.0624 + 0.2054\frac{\Omega_K}{\Omega_m(1+z_{ta})}. \quad (33)$$

In general case the $\delta_{ta}(z_{ta})$ is evaluated by the sequence of equations (16), (30), (31), (26), (32), (23) and (24). The dependences of values δ_{ta} and δ_{min} on the cosmological parameters and redshift z are shown in Figs. 3-4. Note some peculiarities in Fig. 3 at $\Omega_m \simeq 0.032$ for $\Omega_K = -0.2$. These peculiarities indicate the approaching the stationary Einstein model in parameter space, where the equality $27\Omega_m^2(1-\Omega_m-\Omega_K) + 4\Omega_K^3 = 0$ is satisfied. These models are excluded from consideration by enforcing finite positive value for Hubble constant H_0, according to observations. The case of small Ω_m was omitted too, as far as it corresponds to the models with bounce, it is beyond this paper scope.

D. The collapse of overdensity

The moment of complete collapse of spherical overdensity, τ_{col}, is defined by condition $x(R) = 0$. At this moment the matter density $\rho(R)$ as well as the magnitude of its relative overdensity $\delta_M(R)$ become infinite, the Eqs. (19)-(21) become singular. Meanwhile the moment of collapse τ_{col} can be easily estimated, because the solution of Eq. (21) is symmetrical with respect to the turnaround point, τ_{ta}. Thus, the moment of collapse is evaluated by

$$\tau_{col} = 2\tau_{ta} = 2\int_0^{x_{ta}} \frac{dx}{(\Omega_m x^{-1} + \Omega_\Lambda x^2 + \Omega_f)^{1/2}}. \quad (34)$$

It is applied usually along with $\Omega_f(R;\tau_{col})$ (Eqs. (16), (17) and (24)) to determine the linear amplitude, $\delta_{col} = \delta_0$, of perturbation which collapses at given τ_{col}:

$$\delta_{col}(\tau_{col}) \equiv \frac{3}{5}\frac{\Omega_K - \Omega_f(R;\tau_{col})}{\Omega_m} D\left(a(\tau_{col})\right). \quad (35)$$

The critical value of amplitude of the perturbation, which undergoes the collapse at given moment of time τ_{col}, is evaluated for any moment of time τ according to

$$\delta_{col}(\tau_{col}|\tau) = \delta_{col}(\tau_{col}) D\left(a(\tau)\right) / D\left(a(\tau_{col})\right). \quad (36)$$

For the cosmology with $\Omega_K = 0$ the formulas (35) and (36) are equivalent to the results presented in [34]. In the simplest case of $\Omega_m = 1$ and $\Omega_K = 0$ the critical amplitude is

$$\delta_{col}(\tau_{col}|\tau) = \frac{3}{5}\left(\frac{3\pi}{2}\right)^{2/3}\frac{a(\tau)}{a(\tau_{col})} \simeq 1.68647\frac{1+z_{col}}{1+z},$$

at $\tau = \tau_{col}$ it acquires the canonical value.

In the models with non-zero Λ-constant and/or the curvature parameter Ω_K, the value of δ_{col} depends on the collapse moment τ_{col}. However, for $z_{col} > 5$, when the influence of Λ-constant is negligible ($\Omega_\Lambda \ll \Omega_m(1+z_{col})^3$, $\Omega_\Lambda \ll \Omega_K(1+z_{col})^2$), the linear amplitude of collapsing perturbation is described by the following asymptotic dependence on z_{col}:

$$\delta_{col}(z_{col}) \simeq \frac{3}{5}\left[\frac{3\pi}{2}\right]^{2/3} + \frac{3}{5}\left(1 - \frac{13}{35}\left[\frac{3\pi}{2}\right]^{2/3}\right)\frac{\Omega_K}{\Omega_m(1+z_{col})} \simeq 1.6865 - 0.0264\frac{\Omega_K}{\Omega_m(1+z_{col})}. \quad (37)$$

Generally speaking, for some particular cosmology the dependence $\delta_{col}(z)$ evaluated at the moment of collapse z_{col} enables to assess the influence of cosmological parameters on the dynamics of perturbation development during the evolution of Universe.

In general case the sequence of Eqs. (16), (30), (34), (26), (35), (36), (23) and (24) must be applied to analyze the influence of cosmological parameters on the value $\delta_{col}(z)$.

The dependences of δ_{col} on the parameters of cosmological model and the redshift of collapse, z, are presented in Figs. 3-4 along with amplitudes δ_{ta} and δ_{min}. One can see, that δ_{col} is less sensitive to parameters in comparison with δ_{ta} and δ_{min}. As a matter of fact, the magnitude of δ_{col} falls within the narrow range $1.55 \le \delta_{col} \le 1.75$ for the wide range of parameters $0.1 \le \Omega_m \le 1$, $0 \le \Omega_\Lambda \le 1$, $-0.4 \le \Omega_K \le 0.4$.

E. Virialization and final parameters of individual spherical halo

Note that true singularity in the center of the perturbation (*i.e.* halo) is never reached, because the falling of particles is never strictly radial, and small-scale inhomogeneities within the cloud induce additional velocities of particles, etc. The process of virialization is far from trivial, however, after the relaxation has finished and dynamical equilibrium has been established the virial theorem provides us with simple relations between the kinetic energy and gravitational potential. For instance, for a spherical relaxed halo the kinetic energy per unit mass is determined by

$$T_{vir}/m = \frac{1}{2}\left\langle v^2\right\rangle_{vir} = \frac{1}{2}r\frac{\partial U_{vir}}{\partial r}.$$

Within ΛCDM cosmology $U_{vir} = U_{\Lambda|vir} + U_{m|vir} = -H_0^2\Omega_\Lambda x_{vir}^2 - H_0^2\Omega_m/x_{vir}$ and the total energy of isolated

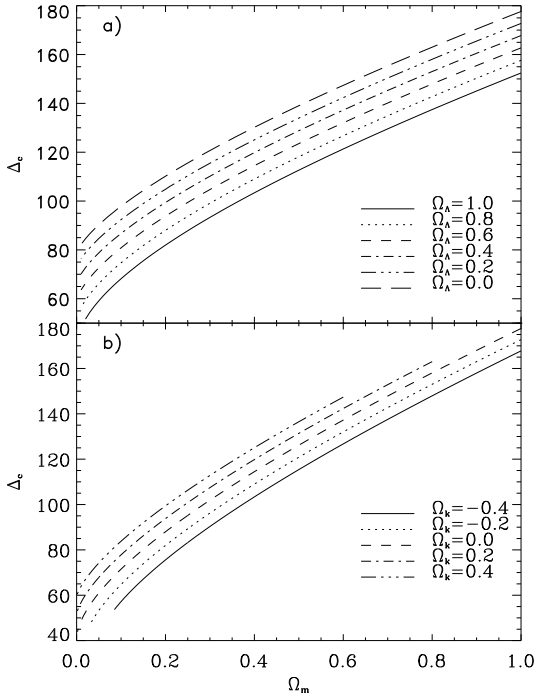

FIG. 5: The dependence of matter density of virialized spherical cloud in units of the critical density at the moment of collapse, Δ_{vc}, on Ω_m in models with fixed Ω_Λ (a) and Ω_K (b).

dark matter cloud is conserved. By comparing the total energy at turnaround point, when kinetic energy is zero ($E_{tot} = U_{ta}$), with one at virialization epoch ($E_{tot} = U_{vir} + T_{vir}$) we get the equality

$$2\Omega_\Lambda x_{vir}^2 + \frac{1}{2}\frac{\Omega_m}{x_{vir}} = \Omega_\Lambda x_{ta}^2 + \frac{\Omega_m}{x_{ta}}. \qquad (38)$$

Taking into account the Eq. (29) for turnaround point we obtain the cubic equation for x_{vir},

$$4\Omega_\Lambda x_{vir}^3 + 2\Omega_f x_{vir} + \Omega_m = 0, \qquad (39)$$

which for overdensity ($\Omega_f < 0$) in cosmology with $\Omega_\Lambda > 0$ has real root

$$x_{vir} = \left(-\frac{2\Omega_f}{3\Omega_\Lambda}\right)^{\frac{1}{2}} \cos\left\{\frac{1}{3}\arccos\left[-\frac{\Omega_m}{8\Omega_\Lambda}\left(-\frac{6\Omega_\Lambda}{\Omega_f}\right)^{\frac{3}{2}}\right] - \frac{2\pi}{3}\right\}. \qquad (40)$$

In $\Omega_\Lambda = 0$ cosmology, as it follows from Eq. (38), the strict equality $x_{vir} = x_{ta}/2$ is obeyed. For $\Omega_\Lambda > 0$ $x_{vir} < x_{ta}/2$, but difference is not large. For example, in fiducial model with $\Omega_\Lambda = 0.7$, $\Omega_m = 0.3$, for perturbation which collapses at current epoch, the relative difference $(\frac{1}{2}x_{ta} - x_{vir})/x_{vir}$ is ~ 0.1 and diminishes with either Ω_Λ decrease or increase of collapse redshift. Therefore, the approximation $x_{vir} \approx x_{ta}/2$ is used in the most applications.

Note, that the value of x_{vir} depends on the local curvature Ω_f and consequently, on the collapse time, t_{col}; the virial mass density, $\rho_{vir} = \rho_m^0 x_{vir}^{-3}$, depends also on t_{col}. It is convenient to represent the virial density in units of critical one at a moment of collapse:

$$\Delta_{vc} = \frac{\rho_{vir}(\tau_{col})}{\rho_{cr}(\tau_{col})} = \frac{\Omega_m H_0^2}{x_{vir}^3(\tau_{col}) H^2(\tau_{col})}. \qquad (41)$$

For the Einstein–de Sitter model ($\Omega_m = 1$, $\Omega_\Lambda = 0$) this ratio does not depend on the collapse moment and equals $\Delta_{vc} = 18\pi^2 \simeq 178$. In the models with $\Omega_\Lambda > 0$ or/and $\Omega_K \neq 0$ it takes different values within the range 40-180, as shown in Fig. 5. In the wide range of parameters $0.05 \leq \Omega_m \leq 1$, $0 \leq \Omega_\Lambda \leq 1$, $-1 \leq \Omega_K \leq 0.95$ it can be estimated with percent accuracy by means of approximation

$$\Delta_{vc} = A - B\log(\Omega_m + C), \qquad (42)$$

where

$$A = 110.89 - 12.91\Omega_\Lambda + 7.92(\Omega_\Lambda)^2 - 0.03/\Omega_m,$$
$$B = -113.28 + 6.84\Omega_\Lambda + 7.13(\Omega_\Lambda)^2,$$
$$C = 0.787 - 0.115\Omega_\Lambda - 0.093(\Omega_\Lambda)^2.$$

The coefficients A, B, C have been determined by the fitting to the exact dependence (41).

III. HALO MERGES, DENSITY PROFILES AND CONCENTRATION PARAMETER

The large-scale structure of Universe seems to be quite complicated, and the N-body numerical simulations are the only technique that strives to provide the complete explanation of it. While the gravitational clustering of dark matter is well-understood, many issues are still relevant to the problem of connection between spatial distribution of dark matter and galaxies. Also, only theoretical analysis can bring some useful insights into the problem. The halo model has been proven to be most fruitful approach for establishing connections between the numerical simulation, theoretical developments and real observed structure of the Universe.

A. Relaxation processes and halo density profile

The violent relaxation is the fastest way for halo to reach the dynamical equilibrium. This type of relaxation is caused by irregular small-scale density inhomogeneities residing in protohalo. The scattering of the individual particles and gravitationally bound groups of particles on such randomly distributed massive inhomogeneities brings the velocity distribution to Maxwell-Boltzmann's one, independent of mass. The same is true for mass

density distribution:

$$\rho(r) = \sum_m mn(m,r) = \sum_m mn_0(m) \exp\left\{-\frac{m\Phi(r)}{kT}\right\} = \rho_s \exp\left\{-\frac{3\Phi(r)}{\sigma_v^2}\right\}. \quad (43)$$

Here, $kT = m\sigma_v^2/3$ is a temperature of particles of mass m, velocity dispersion σ_v depends neither on mass nor radius of particles, $\rho_s = \sum_m mn_0(m)$ is characteristic mass density,

$$\Phi(r) = G\int \frac{M(r)}{r^2}dr, \quad M(r) = 4\pi \int_0^r \rho(r)r^2 dr. \quad (44)$$

Rewriting Eqs. (43) in the differential form

$$\frac{d}{dr}\ln(\rho/\rho_s) = -\frac{3G}{\sigma_v^2}\frac{M(r)}{r^2}, \quad (45)$$

and assuming $\rho(r) = \rho_s(r/r_s)^{-\gamma}$, where r_s is some characteristic radius, we get $\gamma = 2$, $\rho_s = (\sigma_v^2/6\pi G)r_s^{-2}$, and eventually the density profile $\rho(r) = \rho_s(r/r_s)^{-2} = (\sigma_v^2/6\pi G)r^{-2}$. This kind of density profile is called isothermal, because the temperature of particles with fixed mass is constant over the volume of halo.

The duration of violent relaxation is estimated as $(G\rho_{Vir})^{-1/2} \sim (200G\rho_{cr})^{-1/2} \sim 3$ Gyrs and it does not depend on the mass of the gravitational system. This explains how the most of collapsed gravitational systems managed to already achieve the state of dynamic equilibrium in our Universe with age of ~ 13.7 Gyrs. However, despite of expectations, the slopes of the density profiles of virialized halos are lower at small radius than isothermal. The numerical simulations of cluster formation, performed by different teams, provide us with the best-fit values for γ, typically varying within the range $1 \leq \gamma \leq 1.5$ [35]. The most probable reason for this is a phenomenon of orbits separation caused by different gravitational action of central irregularities on the collisionless particles which move in orbits with different eccentricity. The example of such irregularity is a temporary increase of the density in the center of protohalo, taking place at the moment t_{col}, when collapsing particles encounter for the first time. In result, the particles with radial orbits lose kinetic energy so the amplitudes of their orbits sharply decrease (see [36] for details). Meanwhile a kinetic energy of a particle with circular orbit increases, thus the eccentricity of the orbit is enhancing. It gives rise to a radial dependence and anisotropy of particles velocities distribution as well as to velocity dispersion [37–39].

In this case, the condition of dynamical equilibrium is represented by the Jeans equation

$$\sigma_r^2\left(\frac{d\ln\rho}{d\ln r} + \frac{d\ln\sigma_r^2}{d\ln r} + 2\beta\right) = -\frac{GM(r)}{r}, \quad (46)$$

where $\beta = 1 - \sigma_t^2/\sigma_r^2$ is parameter of anisotropy, σ_t and σ_r are respectively the tangential and radial velocity dispersions, and $\sigma^2 = \sigma_t^2 + \sigma_r^2$.

A universal linear relation between the local radial density slope, $\alpha(r) = d\ln\rho/d\ln r$, and the local velocity anisotropy, $\beta(r)$, is identified in [40], for the set of different systems at equilibrium. According to the relation, as the anisotropy decreases towards the center of halo, the slope of its density profile decreases too. Speaking more generally, the conclusion is that the emergence of anisotropy in velocity dispersion is accompanied by a change in the slope of density profile.

Another possible reason for non-isothermal profile is so-called slow relaxation. This type of relaxation is driven by interactions of close pairs of particles, and results in equalizing the temperatures of particles of different masses. Hence, more massive particles have smaller velocity dispersions and appear to be more condensed in comparison to the less massive particles, in accordance with Boltzmann distribution

$$n(m,r) = n_0(m)\exp\left\{-\frac{m\Phi(r)}{kT}\right\}. \quad (47)$$

This phenomenon known as a mass separation. The manifestations of slow relaxation vary with particle distribution over masses, often it is a decrease of γ. In a gravitational system containing N particles with equal or close masses the duration of slow relaxation is larger than duration of violent relaxation by factor of $N/\lg(N)$. For a galaxy cluster consisting of $N \sim 10^3$ similar galaxies or for a galaxy consisting of $N \sim 10^{10}$ stars this factor is very large, therefore the duration of slow relaxation for such systems exceeds the age of the Universe, ~ 13.7 Gyrs. Nevertheless, in a very heterogeneous system containing particles of different masses the mass separation can really be a case, especially if violent relaxation is neither complete nor sufficient.

In N-body cosmological simulations the particles are usually assigned with the same mass, although due to hierarchical clustering of cold dark matter a large number of gravitationally bound subsystems emerge which can be considered as particles of different masses. The distribution of these subsystems, or subhalos, over the masses is far from homogeneous and poorly constrained in range. If violent relaxation can not provide the efficient scattering during protohalo collapse, it results in smaller velocities of the final subhalos. Thus, the mass separation does occur in halos causing the decrease of slope of profiles.

The halo formation is not finished with virialization. The process of merging gradually changes the statistics of halos, also the mass of a halo increases. The merging process is permanent, although the intensity of merging decreases during expansion of the Universe. Thus, the total mass and radius of a halo are functions of time. Less massive halos are trapped from surroundings by central massive halo, they appears to have more energy so they are located at larger distances from the center of system.

Such spatial separation of collisionless particles of different energies is possible only in inhomogeneous gravitational field which is constant or slowly changing in time. This field can be provided by central part of halo, which is left almost untouched after virialization. The shaping of halos in expanding Universe visually recalls the emergence of islands when the level of the surrounding water is gradually dropping. Due to permanent processes of merging, a halo has no sharp boundaries to separate it from environment. Thus, the slope of density profile is $\alpha \leq 3$ at the outskirts of halo.

As commonly adopted, halo density profile is described by simple general expression, $\rho(r) = \rho_s(r/r_s)^{-\gamma}(1 + r/r_s)^{\gamma-\alpha}$, with constraints on parameter found by [35] to be $2.5 \leq \alpha \leq 3$. The characteristic radius r_s specifies the distance, at which the slope of density profile changes. We use universal NFW density profile henceforth, proposed in [41], this is a special case of general profile, with values of slopes fixed as $\gamma = 1$ and $\alpha = 3$:

$$\rho(r) = \frac{\rho_s}{(r/r_s)(1 + r/r_s)^2}. \quad (48)$$

For this density profile the total halo mass diverges logarithmically with r. Therefore we must limit the size of each halo by some finite radius.

B. Statistics of halos

The definition of halo is a matter of convention. Here, the mass of halo is defined as a mass of all matter within the volume of radius r_{vir}. The quantity r_{vir} is defined as a radius of sphere the mean internal density of which equals 200 times the value of the critical density. The mass of the halo is denoted by M_{200}. The mass of halo, constrained by sphere with mean internal density equal to Δ_{vc} times the critical one is denoted by M_Δ. Sometimes the mass of halo is defined with factor of 180 times the critical density, mass is denoted by M_{180} in such case. The index is omitted when the choice of definition is clear from context.

The ratio of radius r_{vir}, used at definition of halo, to the quantity r_s is called concentration parameter (or just concentration) and denoted as c. Depending on the definition of r_{vir}, the concentration is appropriately indexed as c_{200}, c_Δ, c_{180}. In order to define the parameters of halo profile ρ_s and r_s, it is quite enough the define the mass of halo and provide the value for concentration.

The concentration for a halo of fixed mass is a stochastic variable, distributed by log-normal law,

$$p(c|m,z)dc = \frac{1}{\sqrt{2\pi}\sigma_c} \exp\left[-\frac{\ln^2[c/\overline{c}(m,z)]}{2\sigma_c^2}\right] d\ln c. \quad (49)$$

In this case the variance of concentration eventually does not depend on the mass of halo ($\sigma_c = 0.2-0.35$, see [42]), whereas the mean value of concentration is a function of mass and redshift.

The dependence of mean value of concentration upon the mass (called just the mass dependence of concentration hereafter) is determined either by analysis of numerical modeling data or inferred by means of analytical methods, see [41, 43, 44]. Since the mass dependence follows from initial power spectrum of matter, therefore the analytical methods seem to be preferable. The changes in mass dependence caused by modifications of shape or normalization of initial power spectrum can be easily taken into account.

Analytical techniques to study the mass dependences of profile parameters are usually based on the treatment of [41]. The simulations indicate on the growth of profile specific density, ρ_s, with decrease of halo mass. The cause of this was suggested in [41], the less massive but highest inhomogeneities tend to collapse earlier. It was assumed also that specific density of halo, ρ_s, is proportional to the matter density of the Universe, given for the moment of collapse, *i.e.*

$$\rho_s = C\Omega_m\rho_{cr}(1 + z_{col})^3, \quad (50)$$

where the proportionality parameter C is determined from modeling.

The collapse time is defined by "ad-hoc" condition. The collapse is assumed to start at the moment of time, when a half of virial mass of the halo consists of progenitors each more massive than a fixed fraction f of final mass M. With Press-Schechter formalism this condition implies

$$\mathrm{erfc}\left\{\frac{\delta_{col}(z_{col}|z) - \delta_{col}(z|z)}{\sqrt{2(\sigma^2(fM|z) - \sigma^2(M|z))}}\right\} = \frac{1}{2}, \quad (51)$$

leading to the equation:

$$\begin{aligned}\delta_{col}(z_{col}|z) &= \delta_{col}(z|z) + C'\sqrt{\sigma^2(fM|z) - \sigma^2(M|z)} \\ &\simeq \delta_{col}(z|z) + C'\sigma(fM|z), \quad (52)\end{aligned}$$

where $\sigma^2(M|z) = \sigma^2(M)(D(z)/D(0))^2$, $\sigma^2(M) \equiv \sigma^2(M|z=0)$. Here, z is the moment of halo observation, $C' \approx 0.7$, the term $\sigma^2(M|z)$ was neglected in comparison with $\sigma^2(fM|z)$. The parameters C and f are evaluated by the data of modeling. From the analysis of simulation data, it was established (see [41]), that the value of parameter $f \approx 0.01$ does not change substantially, meanwhile the value of parameter $C \propto 10^3$ is quite sensitive to the changes in parameters of background cosmological model and/or initial power spectrum.

Since the parameters C and f have been defined, the specific density of halo, ρ_s, can be estimated from the Eqs. (52) and (50), in order to evaluate other halo parameter r_s for given the halo mass M. Such treatment lacks the explicit analytical expression for dependence $\delta_{col}(z_{col}|z)$, it ought to be computed for each cosmology separately. Therefore it had been proposed in [43] to simplify the equation (52):

$$\sigma(fM_\Delta|z_{col}) = 1.686, \quad (53)$$

$f = 0.01$. Also they had proposed the simple approximation to calculate the concentration $c_\Delta = K(1+z_{col})/(1+z)$, where the value for constant $K = 4$ is estimated from numerical modelling.

As it was shown in [44], the abovementioned treatment is applicable to the estimation of concentration by power spectra in CDM cosmology, however it not so for Warm Dark Matter (WDM) cosmology. The wrong dependences follow for the power spectra of warm dark matter, which predict the decrease of power at smaller scales. The simulations involving initial power spectrum of WDM indicate the increase of concentration with increase of the mass, whereas for the CDM on the contrary the concentration decreases with mass growing.

Since the slope of power spectrum has the same behavior as the slope of dependence of concentration on the mass, it was proposed in [44] to replace the Eqs. (52) and (53) with the following:

$$\sigma_{eff}(M_s|z_{col}) = C_\sigma^{-1},$$
$$\sigma_{eff}(M|z) = \sigma(M|z)\left(-\frac{d\ln\sigma(M)}{d\ln M}\right), \qquad (54)$$

where $C_\sigma \approx 28$, the mass M_s is determined within the radius $r_{max} = 2.17r_s$, at which the rotational velocity of a particle has a maximum for NFW profile. The following estimation has been proposed for the concentration:

$$c_\Delta = \left(\frac{\Delta_{vc}(z_{col})\cdot\Omega_m(z)}{\Delta_{vc}(z)\cdot\Omega_m(z_{col})}\right)^{1/3}\frac{1+z_{col}}{1+z}. \qquad (55)$$

This approximation has an obvious drawback, the z_{col} should be known *a priori*. It is the major obstacle, as the collapse time ought to be computed numerically as root of non-linear equation. We propose to overcome it by altering a few basic assumptions. First, we assume, that specific density of halo is determined primarily by the collapse of quite homogeneous central region of protocloud. The rest of the halo is formed afterwards around this core by the collapse of outer shells. The boundary of the core is defined as the radius, at which the density profile changes its slope, so the mass of the core, M_c, is confined within these edges. The accurate determination of this boundary seems to be impossible, therefore we assumed the mass of core to correspond to the mass of halo with the radius $r_c = \beta r_s$, where $\beta = 0.5$. Thus, the value of mean internal density within the radius r_c corresponds to the density at the moment when dynamical equilibrium is established.

Given this, we can postulate

$$M_c = \frac{4}{3}\pi\rho_{vir}(z_{col})r_c^3 = \frac{4}{3}\pi\Delta_{vc}(z_{col})\rho_{cr}(z_{col})\beta^3 r_s^3, \quad (56)$$

were $\rho_{cr}(z_{col})$ is the critical density at the moment z_{col}. On the other hand, integration of the density profile (48) yields

$$M_c = 4\pi\rho_s r_s^3\left[\ln(1+\beta) - \frac{\beta}{1+\beta}\right]. \qquad (57)$$

Total mass of the halo is

$$M = 4\pi\rho_s r_s^3\left[\ln(1+c) - \frac{c}{1+c}\right]$$
$$= M_c\frac{\ln(1+c) - c/(1+c)}{\ln(1+\beta) - \beta/(1+\beta)}, \qquad (58)$$

where c is halo concentration.

At the next step, in order to evaluate the specific density of halo, ρ_s, the new condition of collapse should be stated, this time for the part of protohalo with mass of M_c within the sphere of radius r_c, at the observation moment. Such condition presumably would bring together the speculations from paper [41] with corrections proposed in [44]. The expressions (54) conforms to the condition

$$\frac{\delta_{col}(z_{col}|z) - \delta_{col}(z|z)}{\sqrt{2(\sigma^2(fM_c|z) - \sigma^2(M_c|z))}} = const, \qquad (59)$$

which is finite value, since $f < 1$ always. To examine the dependence of concentration on the slope and amplitude of power spectrum as found in [44], the term $\sigma^2(M)$ in Eq. (52) must be taken into account. Moreover, in the case of WDM we have one more reason to keep the term $\sigma^2(M)$ in the equation, since the WDM manifests itself in a slow change of r.m.s. of $\sigma^2(M)$ at small values of mass. Thus, in general case the previous approximation is not valid. Assuming the value of f to be close to unity, the Eq. (52) can be approximated as

$$\delta_{col}(z_{col}|z) \approx \delta_{col}(z|z) + C'\left[-\frac{d\sigma^2(M_c)}{d\ln M_c}(1-f)\right.$$
$$\left. - \frac{1}{2}\frac{d^2\sigma^2(M_c)}{d\ln M_c^2}(1-f)^2 - \ldots\right]^{1/2}\frac{D(z)}{D(0)}. \qquad (60)$$

Due to monotonous dependence of $\sigma^2(M)$ on $\ln M$ the high-order derivatives may be omitted, and

$$\delta_{col}(z_{col}|z) \simeq \delta_{col}(z|z) + g\left[-\frac{d\sigma^2(M_c)}{d\ln M_c}\right]^{1/2}\frac{D(z)}{D(0)}, \quad (61)$$

where g is a constant, the value of which can be drawn from simulations.

To confront the Eq. (61) with that of [44], the approximation $\delta_{col}(z_{col}|z) = \delta_{col}(z_{col}|z_{col})D(z)/D(z_{col}) \simeq 1.686D(z)/D(z_{col})$ is used, and the term $\delta_{col}(z|z)$ is dropped as $z_{col} \gg z$ and $\delta_{col}(z_{col}|z) \gg \delta_{col}(z|z)$ for most of observed halos. With these assumptions taken into account, the Eq. (61) is rendered to

$$\frac{D(z_{col})}{D(0)}\sigma_{eff}(M_c) = (\sqrt{2}g/1.686)^{-1},$$
$$\sigma_{eff}(M_c) = \sigma(M_c)\left(-\frac{d\ln\sigma}{d\ln M_c}\right)^{1/2}. \qquad (62)$$

The comparison of Eq. (62) with Eq. (54) reveals apparent difference, namely the powers of derivatives, 1/2

in (62) versus 1 in (54). By the way, the values of constants $\sqrt{2}g/1.686$ and C_σ are not necessary equal, whereas the masses M_c and M_s are defined with spheres with different radii, $r_c = 0.5r_s$ and $r_{max} = 2.17r_s$ respectively. We propose to favor Eq. (61), it is proved to be plausible and well-motivated, comes from condition of [41], whereas the Eq. (54) is based mostly on intuition.

At the next step we have to estimate the parameters of density profile, so that the relation between the critical amplitude $\delta_{col}(z_{col}|z)$ and relative density of virialized perturbation $\Delta_{vc}(z_{col})$ should be found. Note, that according to the definition $\Delta_{vc}(z_{col}) = \Omega_m x_{vir}^{-3}(H(z_{col})/H_0)^{-2}$, where $(H(z_{col})/H_0)^2 = \Omega_m(1+z_{col})^3 + \Omega_K(1+z_{col})^2 + \Omega_\Lambda$, x_{vir} is given by (39).

The $\Omega_f(z_{col})$, local curvature within perturbation collapsing at the moment z_{col} can be expressed via critical amplitude $\delta_{col}(z_{col}|z)$ due to the Eq. (36),

$$\Omega_f(z_{col}) = \Omega_K - \frac{5}{3}\Omega_m \frac{\delta_{col}(z_{col}|z)}{D(z)}. \qquad (63)$$

Further, by evaluating the critical amplitude $\delta_{col}(z_{col}|z)$ for given mass M_c with formula (61), the parameter of profile r_s as a function of M_c can be found, on the base of Eqs. (39) and (63), above-mentioned definitions and Eq. (56),

$$r_s = \frac{x_{vir}}{\beta}\left(\frac{(M_c/10^{12}h^{-1}M_\odot)}{1.163\Omega_m}\right)^{1/3}. \qquad (64)$$

The specific density of halo, ρ_s, is evaluated by Eq. (57). The estimation of halo mass can be carried out given the known density profile and additional condition. However, it is more common to evaluate not just r_s and ρ_s, but the concentration as a function of halo mass.

Since the ratio of mean density of halo to specific density is a function of concentration,

$$\frac{\rho_{halo}}{\rho_s} = \frac{3M}{4\pi r_{vir}^3 \rho_s} = \frac{3}{c^3}\left[\ln(1+c) - \frac{c}{1+c}\right], \qquad (65)$$

so the concentration is a function of these densities ratio [18]:

$$c \simeq \left[\frac{2}{3}\frac{\rho_{halo}}{\rho_s} + \left(\frac{1.1}{2.0}\frac{\rho_{halo}}{\rho_s}\right)^{0.387}\right]^{-1}. \qquad (66)$$

It is convenient to express the specific and mean densities of halo in units of critical density, *i.e.* $\Delta_{sc} \equiv \rho_s/\rho_{cr}$ and $\Delta_{hc} \equiv \rho_{halo}/\rho_{cr}$, or in units of mean density of matter, as $\Delta_{sm} \equiv \rho_s/\overline{\rho}_m$ and $\Delta_{hm} \equiv \rho_{halo}/\overline{\rho}_m$ correspondingly. Thus, $\rho_{halo}/\rho_s = \Delta_{hc}/\Delta_{sc} = \Delta_{hm}/\Delta_{sm}$. According to the condition, used to define the halo radius r_{vir}, one of the values, either Δ_{hc} or Δ_{hm}, should be constant for all halos, meanwhile either Δ_{sc} or Δ_{sm} is evaluated by formulas:

$$\Delta_{sc} = \frac{\Omega_m}{x_{vir}^3}\frac{H_0^2}{H^2(z)}\frac{\beta^3/3}{\ln(1+\beta) - \beta/(1+\beta)}, \qquad (67)$$

$$\Delta_{sm} = \frac{1}{x_{vir}^3}\frac{1}{(1+z)^3}\frac{\beta^3/3}{\ln(1+\beta) - \beta/(1+\beta)}. \qquad (68)$$

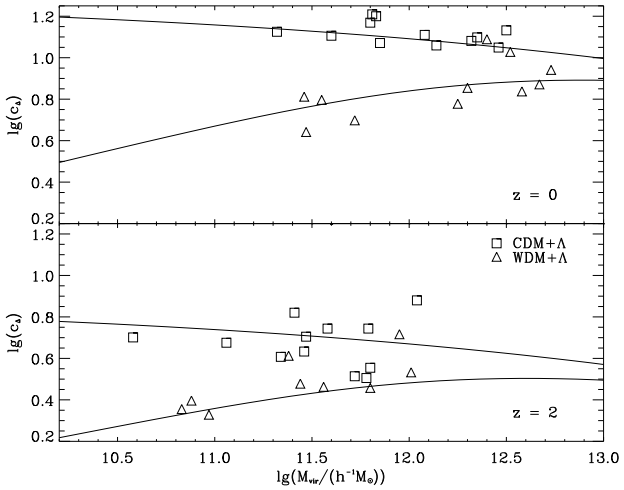

FIG. 6: The dependence of concentration c_Δ on the mass M_{vir}. The squares represent the data for CDM, and the triangles do for WDM, both are borrowed from modeling of [44]. Top panel is plotted for current moment of time, $z = 0$, and the bottom one is for $z = 2$. Solid lines represent our calculations.

The halo mass was calculated by Eq. (58). With analyzing the numerical simulations, we get $g \approx 6.7$.

The results of calculations of concentration c_Δ are represented in Fig. 6, as dependence on the mass M_{vir}. The data of simulation by [44] are plotted for comparison, for cosmology with $\Omega_m = 0.3$, $\Omega_\Lambda = 0.7$, $h = 0.65$ and $\sigma_8 = 0.9$, both for CDM and WDM. The dependence is presented for $z = 0$ and $z = 2$. As it is shown, the concentration grows with the increase of z_{col}. Thus, for older halos concentration is larger than for younger ones. For the ΛCDM cosmology the halos of smaller masses are formed in first turn, subsequently they have larger concentration. For the ΛWDM cosmology the halos with smaller masses can be formed later, thus they have the smaller value of concentration.

The evaluated dependence of halo concentration, c_{200}, on the mass, M_{200}, is represented by solid lines in Fig. 7. The triangles represent the data from paper [45], taken for cosmological model with parameters provided in [46] by 5-year data release of WMAP: $\Omega_\Lambda = 0.721$, $\Omega_m = 0.279$, $\Omega_b = 0.0441$, $h = 0.719$, $\sigma_8 = 0.796$ and $n_s = 0.963$. Three plots represent the data calculated for the values of redshifts varying $z = 0, 1, 2$. As it can be seen, our calculations agree quite well with the data of modeling at all redshifts.

IV. MASS FUNCTIONS AND POWER SPECTRA OF HALOS

An analytical approach for mass function of clusters of galaxies had been suggested in pioneering paper of [47], which is based on the model of spherical collapse and

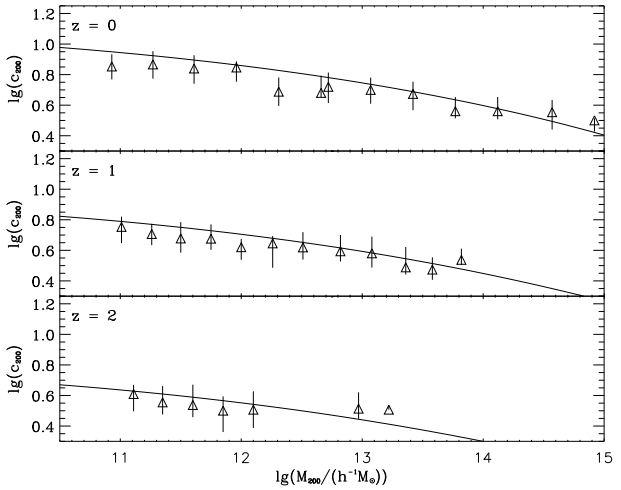

FIG. 7: The dependence of concentration, c_{200}, on the mass M_{200}. The triangles represent the modelling by [45]. The solid lines represent our results. The plots are given for the redshifts $z = 0, 1, 2$ in downward order.

identifies the halos with the peaks of an initially Gaussian field of density perturbations. This so-called Press-Schechter formalism produces the halo mass function to describe the distribution of halos over their masses. The approach was refined and extended afterwards in [48–50] to allow for the merger histories of dark matter halos. The process of halo merging is assumed to be hierarchical at the large scales, and described with characteristic collapsing mass scale $m(t_{col})$ with r.m.s. of density perturbations $\sigma(m) = \delta_{col}(t_{col})$. This mass grows with time through merging of halos and in distant future it will approach asymptotically the limit value m_∞ at which $\sigma(m_\infty) = \delta_{min}$. For cosmology with $\delta_{min} = 0$ the clustering of dark matter has no end in meaning that all halos of the Universe will merge in far future.

A. Halo mass function

Authors of [48] have argued that Press-Schechter mass function $n(m, z)$, the number density of gravitationally bound objects with masses m at redshift z, satisfies the condition

$$\nu F(\nu) \equiv \frac{m^2 n(m,z)}{\overline{\rho}_m} \frac{d\ln m}{d\ln \nu} = \sqrt{\frac{\nu}{2\pi}} \exp\{-\nu/2\}, \quad (69)$$

where $\nu \equiv (\delta_{col}(t_{col})/\sigma(m))^2$ and $\overline{\rho}_m$ is the background matter density.

The mass function of Press-Schechter is qualitatively correct however it disagrees with the data of N-body simulations in some details. Treating the collapsing perturbations as ellipsoidal rather than spherical diminishes the discrepancies (see [51]). Indeed, by assuming the average ellipticity of perturbation with mass m and amplitude δ to be $e_{mp} = (\sigma(m)/\delta)/\sqrt{5}$, a simple relation was obtained in [52] to connect ellipsoidal and spherical collapse thresholds

$$\delta_{ec}(m, t_{col}) = \delta_{col}(t_{col}) \left(1 + 0.47 \left[\frac{\sigma(m)}{\delta_{col}(t_{col})}\right]^{1.23}\right). \quad (70)$$

Also, the excursion set model was used in [48] to estimate the mass function associated with ellipsoidal collapse

$$\nu F(\nu) = A(p)\left(1 + \nu^{-p}\right)\sqrt{\frac{\nu}{2\pi}} \exp\{-\nu/2\}, \quad (71)$$

where as before $\nu \equiv (\delta_{col}(t_{col})/\sigma(m))^2$, a parameter $p \simeq 0.3$ and function $A(p) \equiv [1 + 2^{-p}\Gamma(1/2 - p)/\sqrt{\pi}]^{-1} \simeq 0.3222$ are determined by requirement that all mass is gathered within halos, *i.e.* the integration of $F(\nu)$ over ν yields unity. In order to match the data of GIF numerical simulations the mass function (71) has been parameterized in [51] as

$$\nu F(\nu) = A(p)\left(1 + (q\nu)^{-p}\right)\sqrt{\frac{q\nu}{2\pi}} \exp\{-q\nu/2\}. \quad (72)$$

The additional parameter q was evaluated as $q = 0.707$, later it was re-determined in [53] to be $q = 0.75$. In the framework of excursion set approach the ellipsoidal threshold associated with such mass function is as follows, see [52]

$$\delta_{eq}(m, t_{col}) = q^{\frac{1}{2}}\delta_{col}(t_{col}) \left(1 + 0.5 \left[\frac{\sigma(m)}{q^{\frac{1}{2}}\delta_{col}(t_{col})}\right]^{1.2}\right). \quad (73)$$

Two different algorithms are commonly used to identify the dark matter halos within data of numerical N-body simulations: the friend-of-friend (FOF) algorithm [54] and the spherical overdensity (SO) finder [55]. The FOF procedure depends on just one free parameter, b, which defines the linking length as $b\overline{n}^{-1/3}$, where $\overline{n}$ is the average particle density. Thus, in the limit of very large number of particles per halo, FOF approximately selects the halo as matter enclosed by an isodensity surface at which $\rho = \overline{\rho}/b^3$. SO algorithm finds the values of the average halo density in spherical volumes of various sizes. The criterion for identifying the halo is equality of the average density in the sphere to certain value $\kappa\overline{\rho}_m$, where $\overline{\rho}_m$ is mean density of matter in sample and κ is a parameter of algorithm. For the NFW density profile these algorithms appear not to be identical as they lead to different dependences of the halo concentration c on halo mass. Nevertheless, very similar halo mass functions have been found in [56], using SO ($\kappa = 180$) and FOF ($b = 0.2$) halo finders.

We refer halo as a gravitationally bound system which has reached the dynamical equilibrium, meanwhile both SO and FOF finders select the groups of close particles regardless of their dynamical properties, halos are treated

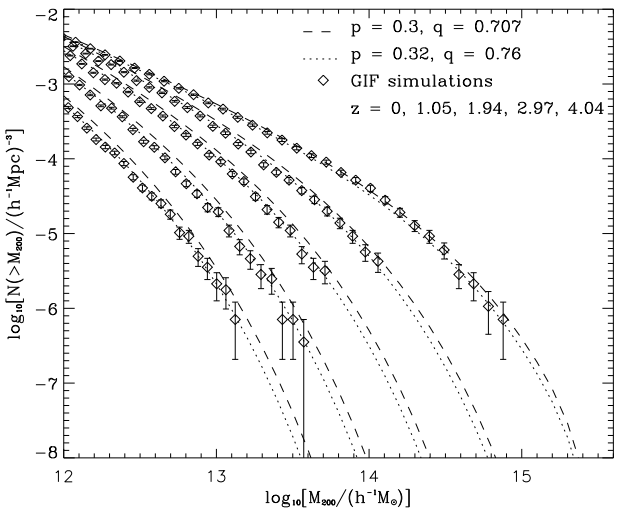

FIG. 8: Halo mass function from N-body numerical simulation by GIF/Virgo collaboration [59] for different redshifts $z = 0, 1.05, 1.94, 2.97, 4.04$. The dashed lines show the Sheth-Tormen approximation with parameters $p = 0.3$ and $q = 0.707$ [51], the dotted lines show the same approximation with modified parameters $p = 0.32$ and $q = 0.76$.

simply as dense regions. To divide such halos into virialized (relaxed) and non-virialized (not relaxed) parts, it was suggested in [57] to assess the dynamical state of each halo processed by FOF algorithm by means of three objective criteria: 1) The substructure mass function f_{sub}; 2) The center of mass displacement $s = |r_c - r_{cm}|/r_{vir}$, and 3) The virial ratio $2T/U$. In [58] the r.m.s. of the NFW fit to the density profile, ρ_{rms}, have been utilized too.

As far as virial density $\rho_{vir} = \rho_{cr}\Delta_{vc} = \overline{\rho}_m\Delta_{vm}$, it seems appropriate to use SO halo-finder with $\kappa = \Delta_{vm} = \Delta_{vc}/\Omega_m$. The equality $\kappa \simeq 180$ is valid for any redshift in flat $\Omega_m = 1$ cosmology (this is close to the $b \simeq 0.2$ for FOF algorithm), meanwhile for ΛCDM cosmology with $\Omega_m = 0.3$, $\Omega_\Lambda = 0.7$ the quantities κ and b depend on redshift: $\kappa \simeq 97/0.3 \simeq 324$ ($b \simeq 0.164$) at $z = 0$ and slowly decrease (increase) to the limit $\kappa \simeq 180$ ($b \simeq 0.2$) at high z. However, as it is shown in [56] the shape of mass function is invariant if we simply identify clusters with a constant linking length, $b = 0.2$, for all redshift and cosmologies.

The halo mass function derived from N-body simulations by GIF/Virgo collaboration is plotted in Fig. 8. The halo catalogs are built from simulation and made available[3]. For each halo, as detected by FOF-algorithm ($b = 0.2$), the catalogs include the mass M_{200}, confined within the central part of halo with overdensity $\Delta_{vm} = 200$ (see [59] for details). The mass rescaling affects slightly the 'observed' mass function. We have re-determined the parameters of Sheth-Tormen approximation to be $p = 0.32$ and $q = 0.76$. As it follows from Fig. 8, the refined parameters provide a better fit for data than ones from [51], $p = 0.3$ and $q = 0.707$. The mass function is defined here as a number density of halos with masses exceeding the specified mass m,

$$N(>m) = \int_m^\infty n(m', z)dm' = \int_m^\infty \frac{\overline{\rho}_m}{m'}\nu F(\nu)\frac{d\ln\nu}{dm'}dm'. \tag{74}$$

Note, that changes in FOF or SO halo finder parameters modify also the total number of detected halos. However, the mass rescaling influences the mass function shape but not the total number of halos.

According to Press-Schechter formalism [47] halos are formed within regions with initial overdensities $\delta \geq \delta_{col}$ because these have already reached a dynamical equilibrium through the collapse. However, for some region to reach overdensity Δ_{vm}, the initial overdensity can be lower than δ_{col}. Given the non-linear overdensity as $\delta_M = 180$ in (27), the corresponding initial overdensity in the units of critical density is calculated as $q^{\frac{1}{2}} \equiv \overline{\delta}/\delta_{col} \simeq 0.95$. Therefore, the applied SO-algorithm ($\kappa = \Delta_{vm}$) marks also as halos non-virialized dense regions formed by growth of perturbations with lower initial overdensities, determined by $q^{\frac{1}{2}}\delta_{col}$ under assumption of spherical symmetry, the value $q < 1$ and depends on Δ_{vm} according to (27). It seems reasonable to assume that the elliptical 'q-threshold' δ_{eq} is directly connected to spherical 'q-threshold' $q^{\frac{1}{2}}\delta_{col}$ through (73) just as the elliptical collapse threshold δ_{ec} is related to the spherical collapse threshold δ_{col} through (70). However the value $q \simeq 0.95^2 \simeq 0.90$ obtained here for $\Delta_{vm} = 180$ differs from the value $q \simeq 0.75$ derived from numerical simulations using FOF ($b = 0.2$) and SO ($\kappa = 180$) algorithms. It is known that large halos are mostly spherical, and hence their mass distribution should be compatible with Press-Schechter mass function. Indeed, if the spherical 'q' barrier $0.95\delta_{col}$ (0.9ν for ν) is used in (69) instead of δ_{col}, a good match is attained to the results of numerical simulations for large ν and hence large masses. However, the Press-Schechter mass function predicts the larger number of halos with smaller than expected masses. The reason is that less massive halos are more elliptical, and therefore according to (70) need larger initial amplitude to form.

B. Subhalo mass function

As it was noted, the clustering of dark matter is a kind of hierarchical process, *i.e.* the halos of small mass have come out first, part of them subsequently are merged to form massive halos. After initial merging the halo progenitors gradually scattered during slow relaxation, and

[3] http://www.mpa-garching.mpg.de/GIF

the most massive even survived within virialized halo as subhalos. A large number of smaller progenitors usually mold a smooth part of halo, *i.e.* diffuse dark matter which is not involved into any substructure. The considerations on the dark matter halo substructure are important to understand the clustering of dark matter on a small scales $\sim 10^3 \div 10^6$ pc [24], internal structure of galaxies [60] and galaxy clusters (see [15–17, 61]). The subhalos may also reveal substructures, consequently sub-subhalos and so on, the algorithm to identify substructures through all levels of this hierarchy was proposed in [27], and applied to determine the mass function from numerical simulations.

The conditional mass function, proposed in [48], provides the description for the merger history of dark matter halos, it can be simply derived from (72) by putting $\nu \equiv [(\delta_{col}(\tilde{z}_{col}) - \delta_{col}(z_{col}))/(\sigma(m) - \sigma(M))]^2$, where M is observed halo mass at z_{col} and $m < M$ is a mass of its progenitor found at some moment $\tilde{z}_{col} > z_{col}$. To adapt this finder for the substructure we assume that $\delta_{col}(\tilde{z}_{col}) = \sigma(m_{rs})$, where m_{rs} is a sort of resolution scale, a limitation up to which the substructure is resolved. So, substructures within subhalos of mass below m_{rs} are not resolved.

To provide best-fit to numerical estimation of subhalo mass function [27], we multiply our conditional mass function by factor of 0.3. It means that halo mass consists only by 30% of subhalos and rest 70% is a diffuse dark matter which not to be associated with any substructure. Hence, we arrive at

$$\frac{dN}{d\ln m} = 0.3 M \nu F(\nu) \frac{d\ln\sigma^2(m)}{dm}, \qquad (75)$$

where $\nu = (1.5\delta_{col})^2/(\sigma^2(m) - \sigma^2(M))$, and $d\ln\sigma^2(m)$ is used instead of term $d\ln\left[\sigma^2(m) - \sigma^2(M)\right]$ because it provides a better accordance when m is close to halo mass M. Note that all estimations of mass from numerical data were carried out for virial overdensity regions with Δ_{vc}.

The subhalo mass function depends on the power spectrum via $\sigma(m)$ and $\sigma(M)$, here the type of dark matter is involved. For warm and hot dark matter the number of low-mass subhalos is expected to be lower in comparison to cold dark matter [62]. The previous approximations proposed for subhalo mass function in [27, 63] do not include such important dependence.

C. The dark matter power spectrum

A process of formation of galaxy as a luminous object consists mainly in baryon matter which undergoes condensing and cooling within potential wells formed by inhomogeneities of dark matter. Therefore, the observable spatial distribution of galaxies should strongly correlate with distribution of dark matter. Since the content of dark matter (≈25%) substantially overwhelms the content of baryon matter (≈5%), so the formation of large-scale structure of Universe is defined primarily by the development of dark matter inhomogeneities.

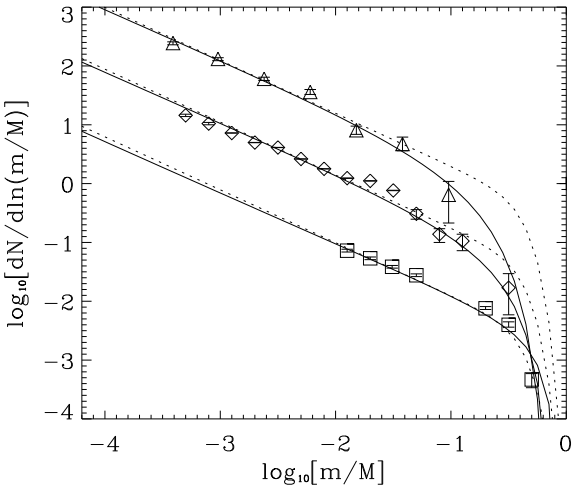

FIG. 9: Subhalo mass function from [27] for three different halo masses – $\log_{10}(M/M_\odot) = 14.25$ (triangles), $\log_{10}(M/M_\odot) = 13.75$ (diamonds) and $\log_{10}(M/M_\odot) = 12.25$ (squares). Subhalo mass functions for halo masses $\log_{10}(M/M_\odot) = 14.25$ and $\log_{10}(M/M_\odot) = 12.25$ are rescaled by 10 up and down respectively. Solid line show our approximation (75) whereas dashed line show the original approximation from [27].

Given that, we need to calculate the characteristics of distribution of dark matter in order to reconstruct the distribution of all matter, *i.e.* the characteristics of observable distribution of galaxies and temperature fluctuations of cosmic microwave background.

1. *Two-point correlation function and power spectrum of discrete and continuous distributions of matter*

The two-point correlation function provides comprehensive statistical description for inhomogeneous spatial distribution of matter. The power spectrum is actually a Fourier transformation of the two-point correlation function, and can be directly drawn from the spatial distribution of matter by means of Fourier-expansion of relative fluctuations of density. In the case of continuous distribution of matter the expansion is following:

$$\begin{aligned}\delta(\vec{r}) &= \frac{\rho(\vec{r}) - \overline{\rho}}{\overline{\rho}} = (2\pi)^{3/2} V^{1/2} \int \delta_{\vec{k}} e^{-i\vec{k}\vec{r}} d^3\vec{k} \\ &= \frac{(2\pi)^{3/2}}{V^{1/2}} \sum_{\vec{k}} \delta_{\vec{k}} e^{-i\vec{k}\vec{r}}, \qquad (76)\end{aligned}$$

here, V denotes some volume of periodicity, the result does not depend on this quantity. The coefficient of expansion can be expressed from (76) in the following man-

ner:

$$\delta_{\vec{k}} = \frac{1}{(2\pi)^{3/2}V^{1/2}} \int \delta(\vec{r}) e^{i\vec{k}\vec{r}} d^3\vec{r}. \quad (77)$$

The squared Fourier amplitude averaged over the different directions of vector $\vec{k}$ is actually what is called the power spectrum, $\mathcal{P}(k) = \left\langle |\delta_{\vec{k}}|^2 \right\rangle$. The two-point correlation function can be derived from known power spectrum,

$$\xi(r) = \langle \delta(\vec{r}')\delta(\vec{r}'+\vec{r})\rangle = \frac{(2\pi)^3}{V}\sum_{\vec{k}} \left\langle |\delta_{\vec{k}}|^2 \right\rangle e^{i\vec{k}\vec{r}}$$

$$= \int d^3\vec{k} \left\langle |\delta_{\vec{k}}|^2 \right\rangle e^{i\vec{k}\vec{r}} = 4\pi \int_0^\infty k^2 dk \mathcal{P}(k) \frac{\sin(kr)}{kr}, \quad (78)$$

as well as variance of the amplitude within the spherical volume of R radius,

$$\sigma^2(R) = <\delta_R^2> = 4\pi \int k^2 \mathcal{P}(k) W^2(kR) dk$$

$$= \int \Delta^2(k) W^2(kR) d\ln k, \quad (79)$$

where $W(x) = 3(\sin(x) - x\cos(x))/x^3$ is a window function for spherical volume.

The quantity $\Delta^2(k) = 4\pi k^3 \mathcal{P}(k)$ is a dimensionless power spectrum. The term "dimensionless" is often omitted, as it is clearly understood from the context of usage. For given correlation function, the power spectrum is evaluated by the following formula

$$\mathcal{P}(k) = \frac{1}{(2\pi)^3} \int d^3\vec{r} e^{-i\vec{k}\vec{r}} \xi(r). \quad (80)$$

The galaxy catalogs (or the data of numerical simulations) involve discrete distributions of galaxies (or particles). In this case the equations (76) and (77) should be recasted with $\rho(\vec{r}) = \sum_i m_i \delta_D(\vec{r} - \vec{r}_i)$, where m_i is the mass of i-th galaxy (particle), $\delta_D(\vec{r} - \vec{r}_i)$ is three-dimensional Dirac function. The Eq. (77) takes the form of

$$\delta_{\vec{k}} = \frac{1}{(2\pi)^{3/2} \langle m \rangle \overline{n} V^{1/2}} \sum_i m_i e^{-i\vec{k}\vec{r}_i}, \quad (81)$$

here $\overline{n}$ is spatially averaged number density of galaxies or particles, $\langle m \rangle = \sum m_i/(\overline{n}V)$ is the mean mass.

The power spectrum is related to the correlation function by relation [64] In such case

$$\mathcal{P}(k) = \frac{\left\langle m^2 \right\rangle}{(2\pi)^3 \overline{n} \langle m \rangle^2} + \frac{1}{(2\pi)^3} \int d^3\vec{r} e^{-i\vec{k}\vec{r}} \xi(r), \quad (82)$$

with $\left\langle m^2 \right\rangle = \sum m_i^2/(\overline{n}V)$. The first term in right-hand side of (82) is a shot noise, denoted by $\mathcal{P}_{shot}$. It corresponds to the case of discrete distribution, when the number density of galaxies (particles) $\overline{n}$ takes large but finite value. At $\overline{n} \to \infty$, *i.e.* for the continuous distribution the Eqs. (82) and (80) converge. The second term in right-hand side of (82) is denoted henceforth as $\mathcal{P}_\xi(k)$ to emphasize the non-random (correlated) nature of distribution. Thus, the Eq. (82) can be written in more compact form, as $\mathcal{P}(k) = \mathcal{P}_{shot} + \mathcal{P}_\xi(k)$.

2. Non-linear power spectrum in halo model

Within halo model the distribution of matter is treated in a mixed, discrete-continuous manner. The matter is segregated into spatially separated halos of different mass, somehow distributed over the space, and the matter distribution within each halo is described by continuous density profile (48). Therefore, the power spectrum is split into two terms, one to describe the distribution of halos, and the second to describe the distribution of matter within individual halo. The splitting can be derived rigorously taking into account that Fourier-amplitudes of density perturbations are (see for details Appendix A)

$$\delta_{\vec{k}} = \frac{1}{\overline{\rho}} \int_0^\infty m \cdot n(m) \delta_{\vec{k}}(m) \overline{y}(m,k) dm. \quad (83)$$

Here $\overline{\rho} = \overline{\rho}_m^0/a^3$ is an average matter density at any moment of time determined by scale factor $a = (1+z)^{-1}$ and $n(m)$ is the number density of halo with mass m drawn from (72) in comoving coordinates.

The function $\overline{y}(m,k)$ is a Fourier-transformation of density profile (48) expressed by explicit analytical form

$$\overline{y}(m,k) = \frac{4\pi}{m} \int_0^{r_{vir}/a} \frac{\sin(kR)}{kR} \rho(Ra) R^2 dR$$

$$= \frac{4\pi\rho_s r_s^3}{ma^3} \left\{ \left[Si\left(\frac{kr_s}{a}(1+c)\right) - Si\left(\frac{kr_s}{a}\right)\right] \sin\left(\frac{kr_s}{a}\right) \right.$$

$$+ \left[Ci\left(\frac{kr_s}{a}(1+c)\right) - Ci\left(\frac{kr_s}{a}\right)\right] \cos\left(\frac{kr_s}{a}\right)$$

$$\left. - \frac{a}{(1+c)kr_s} \sin\left(c\frac{kr_s}{a}\right) \right\}, \quad (84)$$

where c is the halo concentration, ρ_s and r_s are parameters of density profile, $Si(x)$ and $Ci(x)$ are integral sine and cosine respectively. The halo profile depends on the physical coordinates, while the power spectrum is associated with comoving coordinates $R = r/a$. The term $4\pi\rho_s r_s^3/m$ can be expressed via halo concentration parameter c using the Eq. (58).

The power spectrum $\mathcal{P}(k|m,m')$ of spatial distribution of halos with given masses m and m', is following

$$\mathcal{P}(k|m,m') = \frac{1}{2}\left\langle \delta_{\vec{k}}^*(m)\delta_{\vec{k}}(m') + \delta_{\vec{k}}(m)\delta_{\vec{k}}^*(m') \right\rangle$$

$$= \frac{\delta_{m,m'}}{(2\pi)^3 n(m)} + \mathcal{P}_\xi(k|m,m').$$

where $\delta_{m,m'}$ is Kronecker symbol, $\mathcal{P}_\xi(k|m,m')$ is Fourier-image of two-point cross-correlation function of halos with masses m and m' (the angle brackets in the left-hand side denote the averaging over the directions of vector $\vec{k}$).

After the series of mathematical transformations, we arrive to

$$\mathcal{P}(k) = \frac{1}{(2\pi)^3\overline{\rho}^2}\int\limits_0^\infty m^2\cdot n(m)|\overline{y}(m,k)|^2dm + \frac{1}{\overline{\rho}^2}\int\limits_0^\infty m\cdot n(m)\overline{y}(m,k)dm \times\int\limits_0^\infty m'\cdot n(m')\overline{y}(m',k)dm'\mathcal{P}_\xi(k|m,m'). \quad (85)$$

The quantity $n(m)$ is a number density of halos having masses m.

With assumption of linearity of perturbations cross-correlation power spectrum can be represented as $\mathcal{P}_\xi(k|m,m') \approx b(m)b(m')\mathcal{P}_{lin}(k)$, the $\mathcal{P}_{lin}(k)$ is the linear power spectrum of spatial distribution of matter, $b(m)$ is the biasing parameter which characterize the skew between distributions of halos of mass m and the matter distribution.

Since the distribution of matter is homogeneous at very large scales, the expression (85) is expected to asymptotically approach zero for small wave numbers k. However, the first term in right-hand side of (85) never diminishes. The reason is that binning of matter into separate halos introduces the noise into the procedure, as inherent for discrete distribution. The expression for noise is derived from the first term at (85) by letting the distribution of halo matter to be homogeneous and substituting of Fourier-image of profile $\overline{y}(k,m)$ by window function $W(kR)$, where $R = (3m/(4\pi\overline{\rho}_m))^{1/3}$. After noise elimination, the final expression for the power spectrum of spatial distribution of dark matter is following:

$$\mathcal{P}(k) = \frac{1}{(2\pi)^3}\int\limits_0^\infty\left(\frac{m}{\overline{\rho}}\right)^2 n(m)\left[|\overline{y}(m,k)|^2 - W^2(kR)\right]dm + \left[\int\limits_0^\infty\frac{m}{\overline{\rho}}b_1(m)n(m)\overline{y}(m,k)dm\right]^2\mathcal{P}_{lin}(k). \quad (86)$$

We use this equation to calculate the power spectrum of dark matter in the wide range of scales and compare it with data from N-body numerical simulations.

Also, the calculations were carried out to confront our estimations with results of Large Box and GIF2 N-body simulations available at Max Planck Institute for Astrophysics in Garching. The simulation team provides data files with coordinates, velocities and identification numbers of particles. All particles have equal mass. The parameters of simulations (total number of particles, box size, mass of particles and smoothing scale) are presented in the Tab. I. The smoothing scale is used to avoid the numerical singularities which arise in consequence of particles proximity, when the numerical errors is difficult to control.

TABLE I: The parameters of Large Box (LB) and GIF2 simulations, available at Max Planck Institute for Astrophysics in Garching (http://www.mpa-garching.mpg.de).

Simul.	Npar	L (Mpc/h)	m_p (M_{sun}/h)	l_{soft} (Kpc/h)
GIF2	400^3	110.0	1.73×10^9	6.6
LB	512^3	479.0	6.86×10^{10}	30

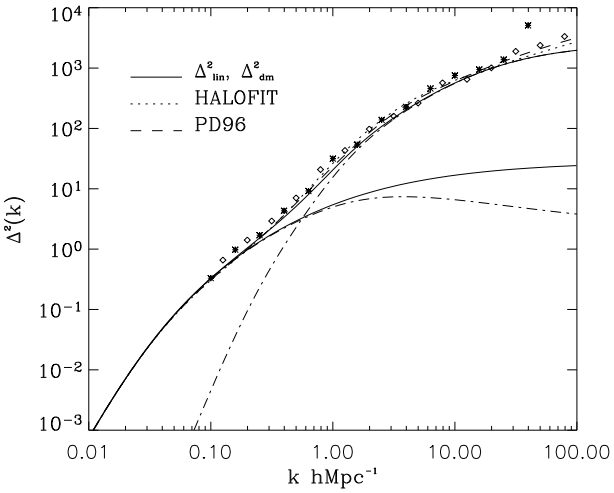

FIG. 10: Dark matter power spectrum obtained from LB (asterisk) and GIF2 (diamonds) simulations. Solid lines represent the primordial linear power spectrum from [65] (lower line) and our predictions for non-linear halo model power spectrum (upper line). Dash-dotted lines show the 'halo-halo' and the 'shot noise' components of the halo model power spectrum. Dotted and dashed lines show PD96 [66] and HALOFIT [67] approximations. The ΛCDM cosmology is used with (Ω_m, Ω_Λ, h, σ_8, n_s)=(0.3, 0.7, 0.7, 0.9, 1).

The higher number density of particles is necessary in order to reproduce the structure at small scales. On the other hand, the larger volume is necessary in order to reproduce the structure on large scales. A pursuit to satisfy both requirements simultaneously leads to the huge numbers of particles, and consequently to the enormous amount of computational efforts. So, usually the separate modelings are carried out, to reproduce the matter distributions at different scales. In our case the data from Large Box simulations cover large volumes, providing thus good reproduction at larges scales, whereas the data from GIF2 simulations is applicable at small scales, having larger average number of particles.

To evaluate the magnitude of power spectrum at given fixed value of wave number k for different fixed direc-

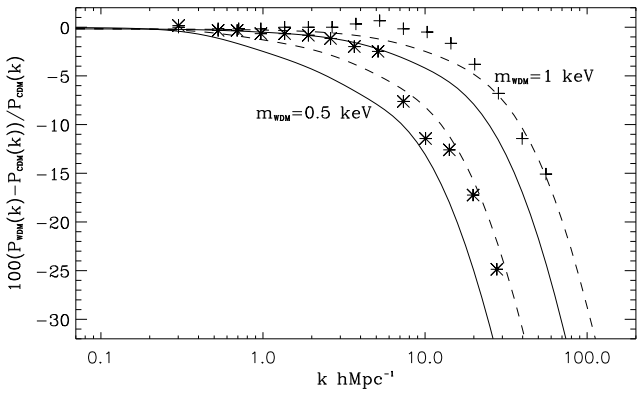

FIG. 11: The difference (percentage) between non-linear power spectra of ΛCDM and ΛWDM models with (Ω_m, Ω_Λ, Ω_b, h, n_s, σ_8)=(0.2711, 0.7289, 0.0451, 0.703, 0.966, 0.809) and two values of WDM particle mass: $m_{wdm} = 1$ keV and $m_{wdm} = 0.5$ keV.

tions of vector $\vec{k}$, denoted by index l, we have estimated the sums of $Sr_l = \sum_i \cos(\vec{k}\vec{r}_i)$ and $Si_l = \sum_i \sin(\vec{k}\vec{r}_i)$, and calculated the power spectra as $\mathcal{P}_l(k) = (Sr_l^2 + Si_l^2)/((2\pi)^3\overline{n}^2 V)$. The net vector was estimated as average over all given directions: $\mathcal{P}(k) = \frac{1}{N}\sum_{l=1..N}\mathcal{P}_l(k)$, where N is total number of given directions. To eliminate the noise, we have precalculated the power spectrum of homogeneous distribution of particles, and substracted this contribution from the power spectrum for the general case of inhomogeneous distribution of particles.

The results of comparison are shown in Fig. 10. As it can be seen, the dark matter power spectrum predicted by halo model, Eq. (86), matches the LB/GIF2 non-linear power spectrum at all scales up to $k \sim 100$ h^{-1}Mpc. Also, the power spectra are shown, calculated by PD96 [66] and HALOFIT [67] approximations based on the previous halo model, of Hamilton et al. [68], scaling relations and fits to numerical simulations. They provide a good fit the LB/GIF2 non-linear power spectrum at all scales as well. In all cases the analytical approximation for linear power spectrum from [65] (lower solid line in Fig. 10) is used, normalized to $\sigma_8 = 0.9$.

Apparently, the non-linear corrections are not essential at $k \leq 0.2$, the power spectrum appears to be linear therein. At smaller scales the non-linear clustering gains domination (dash-dotted line in Fig. 10), and exceeds by amplitude the linear power spectrum. Both our approximation (86) and HALOFIT reproduce such behavior equally good. Consistency of our power spectrum estimation to numerical simulations data and HALOFIT approximation proves the plausibility of our approach, and, on the other hand, gives a deep insight into the process of dark matter clustering and foundations of HALOFIT approximation, which is widely used.

To verify the applicability of our halo model in case of the WDM, we have confronted the non-linear power spectra estimations with the results of numerical simulations from [69]. The initial distribution of warm dark matter particles was generated by following linear power spectrum of density perturbations

$$\mathcal{P}_{lin}^{(wdm)}(k) = \mathcal{P}_{lin}^{(cdm)}(k)\left[\left(1+(\alpha k)^{2\nu}\right)^{-5/\nu}\right]^2, \qquad (87)$$

where[4] $\nu = 1.12$. The parameter α depends on the mass of WDM particles, m_{wdm}, their density, Ω_{wdm} and Hubble parameter as

$$\alpha(m_{wdm}) = 0.049\left(\frac{1keV}{m_{wdm}}\right)^{1.11}\left(\frac{\Omega_{wdm}}{0.25}\right)^{0.11}\left(\frac{h}{0.7}\right)^{1.22}$$

(see also [70] and [71]).

We have computed the non-linear power spectrum of matter density perturbations (86) at $z = 0.5$ for ΛCDM and ΛWDM cosmologies with (Ω_m, Ω_Λ, Ω_b, h, n_s, σ_8)=(0.2711, 0.7289, 0.0451, 0.703, 0.966, 0.809) and two different masses of warm dark matter particles, m_{wdm}, as 1 and 0.5 keV, the same values for which the N-body simulations have been accomplished in [69]. The Fig. 11 represents the relative discrepancies (in percents) between non-linear power spectra of cold and warm dark matter (solid lines), the corresponding spectra calculated from simulations are plotted along (Fig. 7 in [69]). Our results reveal qualitative consistency with simulations however quantitative differences are still noticeable [5].

Note the discrepancy in case of warm dark matter halo model [72], depicted by green line in the bottom panels of Figure 7 in paper [69], are also suppressed in comparison with numerical simulation and seems to be closer to our results. It implies that for WDM models new independent numerical simulations are required to obtain more robust statistics as well as the case should be re-analyzed in the framework of halo model. Indeed, the amplitude of power spectrum is very sensitive to dependence of halo concentration parameter on mass of halos, Eqs. (84) and (86), unfortunately this kind of sensitivity can be verified only by high-resolution numerical models (see also discussions in [44, 72]).

D. The galaxy power spectrum

As the baryon gas falls into potential wells of virialized dark matter halos and subhalos it has been heated to virial temperature of $T = \frac{1}{2}\mu m_p v_{vir}^2/k_B \approx 2\times 10^4\mu_{0.6}(M/10^8 M_\odot)^{2/3}[(1+z)/10]$ K, where $\mu = 0.6\mu_{0.6}$ is a mean molecular mass of post-shock gas, and M is

[4] There is a typo in e-print version of paper [69] arXiv:1107.4094v2 in formula (1): the right-hand side expression for $T^2(k)$ must be squared (private communication with authors)

[5] For the WDM initial power spectrum (1) from arXiv:1107.4094v2 (the square degree in the right-hand side of expression (87) is omitted here) the quantitative accordance is essentially better (dashed lines).

the mass of halo or subhalo progenitors. The temperature of baryon matter gradually decreases afterwards due to the cooling processes (see [5]). It results in fragmentation to smaller clumps with Bonnor-Ebert mass, $M_{BE} \simeq 700 M_\odot (T/200\mathrm{K})^{3/2}(n_b/10^4\mathrm{cm}^{-3})^{-1/2}$, where n_b is the total number density of baryon particles. At the final stage of this fragmentation the stars and galaxies are formed (see [5] and [4] for details). Since formation of galaxies is driven by gravity of dark matter, the spatial distribution of galaxies tracks the spatial distribution of dark matter. In other words, the fluctuations of dark matter density $\delta_{DM}(\vec{r}) = \rho_{DM}(\vec{r})/\overline{\rho}_{DM} - 1$ correlate with fluctuations of galaxy number density $\delta_g(\vec{r}) = n_g(\vec{r})/\overline{n}_g - 1$. The galaxy number density fluctuations have following Fourier amplitude in halo model,

$$\delta_{g|\vec{k}} = \frac{1}{\overline{n}_g} \int\limits_{m_{min}}^{\infty} \langle N_g|m\rangle \, n(m) \delta_{\vec{k}}(m) \overline{y}_g(k,m) dm \qquad (88)$$

(see Appendix B for details). Here $\langle N_g|m\rangle$ is a mean number of galaxies in halo with mass m, $\overline{y}_g(k,m)$ is a Fourier-transform of galaxy number density profile and m_{min} denotes the lowest limit for halo mass below which no galaxies are formed. Such limit naturally comes from degrading efficiency of star formation in halos of low mass [17] and conditions imposed on the sample of galaxies (see [25, 26]).

The considerations of previous subsection are summarized in following the galaxy power spectrum:

$$\begin{aligned} \mathcal{P}_g(k) = & \frac{1}{(2\pi)^3} \int\limits_{m_{min}}^{\infty} \left(\frac{\langle N_g|m\rangle}{\overline{n}_g}\right)^2 n(m) \\ & \times \left[|\overline{y}_g(m,k)|^2 - W^2(kR_g)\right] dm \\ & + \left[\int\limits_{m_{min}}^{\infty} \frac{\langle N_g|m\rangle}{\overline{n}_g} b_1(m) n(m) \overline{y}_g(m,k) dm\right]^2 \mathcal{P}_{lin}(k), \end{aligned} \qquad (89)$$

where $R_g = \left(3\langle N_g|m\rangle/(4\pi\overline{n}_g)\right)^{1/3}$. The resulting equation is similar to the corresponding expression for the galaxy power spectrum from [22]. The difference is caused by elimination of the noise as described above. Also the term $\langle N_g|m\rangle^2$ has been obtained instead of $\langle N_g(N_g-1)|m\rangle$ in [22]. For large-mass halos the term $\langle N_g|m\rangle$ is large, and it seems appropriate to assume the probability distribution $p(N_g|m)$ to be one of Poisson. In this case $\langle N_g|m\rangle^2 \approx \langle N_g(N_g-1)|m\rangle$. However, this equation is not valid for low-mass halos.

As it has been outlined in [16], galaxies within halo usually are disposed around the center (central galaxy) and within each of its subhalos (satellite galaxies). This gives a clue to find out how galaxies are distributed over the halo and how it is connected to the substructure. Massive halos usually undergo the violent relaxation. In such case, as follows from Eq. (43), for the number density of the satellite galaxies in halo the following equation is appropriate

$$\begin{aligned} n_{sg}(r) = & \sum_{m \geq m'_{min}} n_{sh}(m,r) = \sum_{m \geq m'_{min}} n_0(m) \exp\left\{-\frac{m\Phi(r)}{kT}\right\} \\ & = n_g^0 \exp\left\{-\frac{3\Phi(r)}{\sigma_v^2}\right\} = \frac{n_g^0}{\rho_s}\rho(r), \end{aligned} \qquad (90)$$

where $n_{sh}(m,r)$ denotes the dependence of the number density of halo particles (subhalos) with mass m on the radial distance.

As above, we assume that galaxies are formed within subhalos with masses $m \geq m'_{min}$, where m'_{min} is less than m_{min} because subhalos usually lose the mass due to tidal deprivation of their outskirts. Baryon matter (stars) are concentrated to the center and more tightly bound than dark matter and therefore is slightly changing, meanwhile dark matter is stripped off. Thus, the subhalo mass at the time of observation is probably a poor tracer for the potential well which determines galaxy properties such as stellar mass or luminosity. A better tracer is the subhalo mass at the time when it falls into the host halo, or its maximum mass over its history. For massive halos with numerous satellites the presence of the central galaxy can be neglected. In such case, as follows from (90), the assumption $\overline{y}_g(m,k) \simeq \overline{y}(m,k)$ is correct. This result agrees with [73], the spatial distribution of satellite galaxies using SDSS spectroscopic and photometric galaxy catalogs is studied therein. They found that satellite profiles generally have a universal form that well-fitted by NFW approximation.

However, as long as low-mass halos possess a small number of galaxies, slow relaxation is also important for them. In result, the profile of satellite galaxy number density generally deviates from the profile of dark matter density. However, such discrepancy is difficult to detect because of large statistical errors in determination of the profile of the galaxy number density in such halos. Let us note that in this case we also can not discard the presence of central galaxy.

The spatial number density of the galaxies is a sum of the halo and subhalo number densities: $n_g(\vec{r}) = n_h(\vec{r}) + n_{sh}(\vec{r})$. The spatial fluctuation of galaxy number density can be thereby split into fluctuations of halo and subhalo numbers densities:

$$\begin{aligned} \delta_g(\vec{r}) &= \frac{n_h(\vec{r}) + n_{sh}(\vec{r})}{\overline{n}_h + \overline{n}_{sh}} - 1 \\ &= \frac{1}{\overline{n}_h + \overline{n}_{sh}} \left[\overline{n}_h \delta_h(\vec{r}) + \overline{n}_{sh}\delta_{sh}(\vec{r})\right], \end{aligned} \qquad (91)$$

where as before the overlines denote averaging in space. Corresponding Fourier amplitude takes the form

$$\begin{aligned} \delta_{g|\vec{k}} &= \frac{1}{\overline{n}_h + \overline{n}_{sh}} \left[\overline{n}_h \delta_{h|\vec{k}} + \overline{n}_{sh}\delta_{sh|\vec{k}}\right] \qquad (92) \\ &= \frac{1}{\overline{n}_h + \overline{n}_{sh}} \int\limits_{m_{min}}^{\infty} \left[1 + \langle N_{sh}|m\rangle \, \overline{y}_{sh}(k,m)\right] n(m) \delta_{\vec{k}}(m) dm, \end{aligned}$$

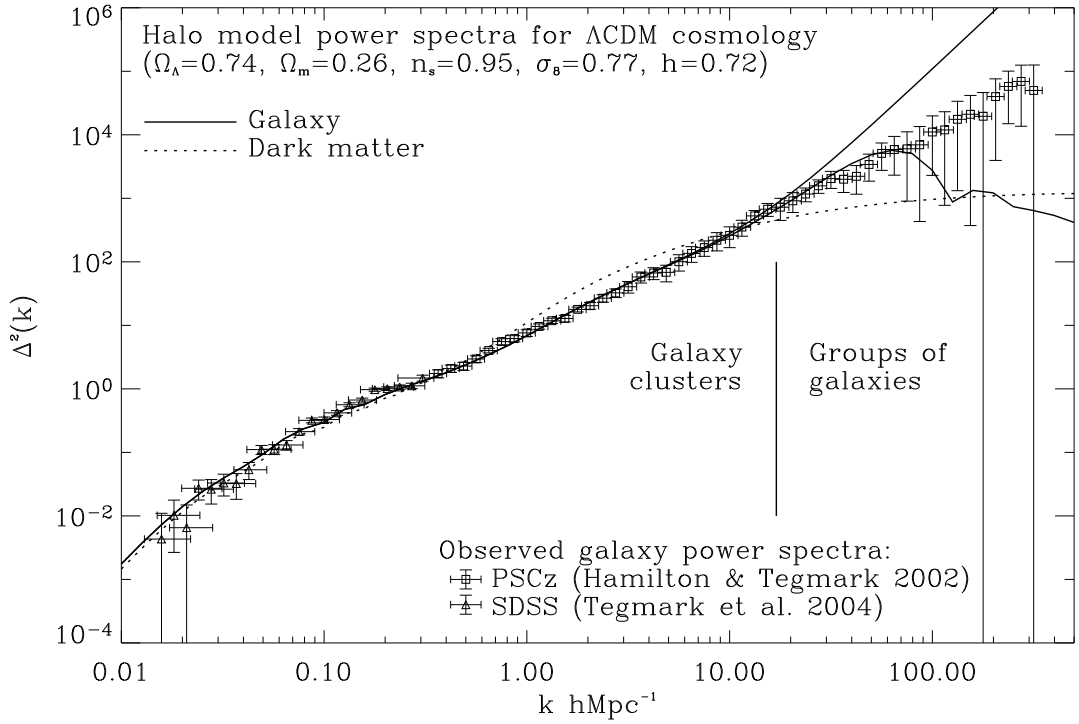

FIG. 12: The halo model galaxy (solid line), dark matter (dotted line) power spectra calculated for ΛCDM cosmology with $(\Omega_m, \Omega_\Lambda, h, \sigma_8, n_s) = (0.26, 0.74, 0.72, 0.77, 0.95)$. The squares and triangles represent the observed galaxy power spectrum drawn from PSCz [25] and SDSS [26] galaxy catalogs respectively.

where $\langle N_{sh}|m\rangle$ is the average number of subhalos confined within the halo of mass m, it equals the number of satellites. Since the average number of galaxies accounts for central galaxy and satellites, therefore $\langle N_g|m\rangle = 1 + \langle N_{sh}|m\rangle$. By comparing Eqs. (88) and (93),

$$\overline{n}_g = \overline{n}_h + \overline{n}_{sh} = \int_{m_{min}}^{\infty} [1 + \langle N_{sh}|m\rangle]\, n(m) dm, \qquad (93)$$

and

$$\overline{y}_g(k,m) = \frac{\langle N_{sh}|m\rangle\, \overline{y}_{sh}(k,m) + \overline{y}_c(k,m)}{\langle N_{sh}|m\rangle + 1}, \qquad (94)$$

where $\overline{y}_{sh}(k,m)$ is a Fourier image of the subhalo number density profile, meanwhile $\overline{y}_c(k,m)$ is a Fourier image of the probability of finding the central galaxy within the halo.

If the central galaxies in all halos with masses m are located strictly in their centers, then $\overline{y}_c(k,m) = 1$. For massive halo, $\langle N_{sh}|m\rangle \gg 1$, so $\overline{y}_g(k,m) \simeq \overline{y}_{sh}(k,m)$, whereas for low-mass halo, $\langle N_{sh}|m\rangle \ll 1$, $\overline{y}_g(k,m) \simeq \overline{y}_c(k,m)$. As follows from Eq. (90) for massive halos we can assume $\overline{y}_{sh}(k,m) \simeq \overline{y}(k,m)$. For simplicity, let us extend this approach to the case of low-mass halo. It should not bring significant errors to $\overline{y}_g(k,m)$ because in the case of $\langle N_{sh}|m\rangle \ll 1$ the central galaxy is dominating, so $\overline{y}_g(k,m) \simeq \overline{y}_c(k,m)$.

To specify the dependence $\langle N_{sh}|m\rangle$ we can use the subhalo mass function (75). In such case the number of satellite galaxies in halo with mass m is

$$\langle N_{sh}|m\rangle = \int_{m'_{min}}^{m} \frac{dN}{dm'} dm', \qquad (95)$$

the masses m and m'_{min} are to be determined within the virial density regions with $\Delta_{vm}\rho_{cr}$.

To provide a direct link to the galaxy sample the CLF [13–15] or CMF [16]) can be also used instead of the subhalo mass function. The CLF, $\Phi(L|m)dL$, yields the average number of galaxies with luminosity $L \pm dL/2$ which reside within a halo of mass m. The CMF, $\Phi(m_*|m)dm_*$, yields the average number of galaxies with stellar masses in the range $m_* \pm dm_*/2$ which reside within halo of mass m. The CMF (as well as CLF) can be split into central and satellite parts so that $\Phi(m_*|m) = \Phi_s(m_*|m) + \Phi_c(m_*|m)$. This allows us to calculate the average number of satellites with a stellar masses exceeding m_* within the halo with mass m (see [16] for details),

$$\langle N_{sh}|m, m_*\rangle = \int_{m_*}^{\infty} \Phi_s(m'_*|m) dm'_*,$$

and the probability of finding the appropriate central

galaxy is

$$\langle N_c|m,m_*\rangle = \int_{m_*}^{\infty} \Phi_c(m'_*|m)dm'_*,$$

where upper limit is assigned with infinity, although it actually does not exceed the halo mass m. To calculate the power spectrum of galaxies, we assume that $\langle N_g|m\rangle = \langle N_{sh}|m,m_*\rangle + \langle N_c|m,m_*\rangle$ and

$$\overline{y}_g(k,m) = \frac{\langle N_{sh}|m,m^*\rangle\, \overline{y}_{sh}(k,m) + \langle N_c|m,m^*\rangle\, \overline{y}_c(k,m)}{\langle N_{sh}|m,m^*\rangle + \langle N_c|m,m^*\rangle}. \quad (96)$$

The average number of galaxies with a stellar mass larger than m_* is given by

$$\overline{n}_g = \int_0^{\infty} \left[\langle N_{sh}|m,m_*\rangle + \langle N_c|m,m_*\rangle\right] n(m)dm. \quad (97)$$

The same calculations are valid for CLF. Hence, the halo model describes the connection between galaxy power spectrum and stellar masses or luminosities of the sample of galaxies.

For example, we have calculated the galaxy power spectrum by using of CMF from [16]. The CMF was used with scatter because it provides better consistency with observations. It was evaluated for ΛCDM cosmology with parameters (Ω_m, Ω_Λ, h, σ_8, n_s) = (0.26, 0.74, 0.72, 0.77, 0.95), so the same parameters were used herein. The CAMB code [74, 75] was used to calculate the initial dark matter power spectrum $\mathcal{P}_{lin}(k)$, with $\Omega_b = 0.05$. For the galaxy power spectrum evaluation the Eq. (96) and Eq. (89) were used with $W(kR_g)$ replaced by

$$\lim_{\mathcal{P}(k)\to 0} \overline{y}_g(k,m) = \frac{\langle N_{sh}|m,m^*\rangle\, W(kR_s) + \langle N_c|m,m^*\rangle\, W(kR_c)}{\langle N_{sh}|m,m^*\rangle + \langle N_c|m,m^*\rangle},$$

where $R_s = \left(3\langle N_{sh}|m,m^*\rangle/(4\pi\overline{n}_g)\right)^{1/3}$ and $R_c = \left(3\langle N_c|m,m^*\rangle/(4\pi\overline{n}_g)\right)^{1/3}$.

We assumed

$$\overline{y}_{sh}(k,m) = \int_{allc} \overline{y}(k,r_s,c')p(c'|m,z)dc'. \quad (98)$$

where $\overline{y}(k,r_s,c)$ denotes the dependence (84) and $p(c|m,z)$ is the function of concentration distribution (49) with variance $\sigma_c = 0.25$.

The calculated galaxy and dark matter power spectra are presented in Fig. 12, along with observed galaxy power spectra obtained from PSCz [25] and SDSS [26] galaxy catalogs.

The upper solid line represents the assumption that the central galaxies in all halos with masses m are located strictly in their centers, so $\overline{y}_c(k,m) = 1$. The lower solid line represents the result for assumption that central galaxies are homogeneously distributed over the spherical volume of radius $1.1r_s$, so $\overline{y}_c(k,m) = W(1.1r_sk)$. We define the lower limit on the stellar masses of the galaxies to be $m_* = 5\times 10^6\ M_\odot$.

Thus, at large scales, $k \le 1$ h^{-1}Mpc, the dark matter and galaxy power spectra coincide, at galaxy cluster scales, $1 \le k \le 20$ h^{-1}Mpc, they are close and start to diverge at smaller scales, $k > 20$ h^{-1}Mpc, where luminous matter is substantially more clustered than dark matter.

V. CONCLUSIONS

The presented semi-analytical treatment is our implementation of halo model capable to describe and interpret the clustering of the matter at the non-linear stage of evolution, both in simulated and observed Universe. Some of basic elements of theory is reviewed and improved to calculate the dark matter and galaxy power spectrum.

At first we have analyzed the evolution of spherical scalar perturbations in different cosmologies for arbitrary initial density profile to find the relations between amplitude of linear perturbations and overdensities at non-linear stages. These relations enable to estimate the moments of turnaround, collapse and virialization of spherical overdensity for any set of main cosmological parameters, Ω_m, Ω_Λ, Ω_K and H_0. The minimal amplitudes are estimated of initial density perturbations δ_{min} which can seed virialized halo in $\Omega_K > 0$ or/and $\Omega_\Lambda > 0$ cosmologies. The exact analytical expressions (30), (32), (35), (40) are suggested as well as analytical approximations (33), (37), (42).

We propose a new technique for computation of halo concentration parameter, c, with phenomenology of halo merging, density profiles and statistical properties taken into account. The simple expression for estimation (66) depends on the relation of the halo overdensity, Δ_{vc} or Δ_{vc}, and corresponding characteristic halo overdensity, Δ_{sc} or Δ_{sc} respectively. This relation is evaluated without computing redshift of halo collapse, z_{col}, by set of equations: (66), (61), (63), (40) and (67) or (68) as well. Such technique has been applied to calculate the concentration parameter for ΛCDM and ΛWDM cosmological models, and the concordance with data of simulations [44, 45] for vast range of halo masses (Figs. 6, 7) has been revealed.

The parameters of Sheth-Tormen approximation for halo mass function were re-evaluated as $p = 0.32$ and $q = 0.76$ (see Fig. 8) to provide best-fit to the data of GIF/Virgo N-body simulations [59] (see Fig. 8). The proposed approximations for subhalo mass function, Eq. (75) match the derived from GIF2 [27] (Fig. 9). It implies that halo mass consists only by 30% of subhalos and the rest 70% is a diffuse dark matter which not to be associated with any substructure. However, we stress that resolving of substructure is limited by a some specified resolution level caused by finite resolution of numerical simulations.

Also, this modified and extended halo model enables to predict the dark matter and galaxy power spectra at small scales up to $k \sim 100$ h^{-1}Mpc by means of semi-analytical methods Eqs. (85), (86), (89). The estimated spectra agree with with non-linear power spectra determined from Large Box and GIF2 N-body simulations (Fig. 10) as well as with estimations by galaxy catalogs PSCz [25] and SDSS [26] (Fig. 12). Moreover, with the assumption on presence of the central galaxies in all halos with masses m ($\overline{y}_c(k,m) = 1$) the technique predicts galaxy power spectrum, matching well the observational one up to $k \sim 20$ h^{-1}Mpc. Meanwhile, when non-central position of most massive galaxies in halos is assumed, ($\overline{y}_c(k,m) = W(1.1 r_s k)$), the predictions agree with the observational data up to $k \sim 80$ h^{-1}Mpc.

The calculated non-linear galaxy power spectrum for ΛCDM cosmology with $(\Omega_m, \Omega_\Lambda, h, \sigma_8, n_s) = (0.26,\ 0.74,\ 0.72,\ 0.77,\ 0.95)$ corresponds to the observational one for lower limitation on the stellar masses of the galaxies $m_* = 5 \cdot 10^6\ M_\odot$. To attain the same level of agreement of the predicted galaxy power spectrum with extracted from galaxy surveys at smaller scales ($k > 80$ h^{-1}Mpc), a new complicated approach for the formation of groups of galaxies must be elaborated.

Despite the ambiguities in the definition of halo, determining of their mass, concentration and substructure, halo model provides a good reproduction of such characteristics of large-scale structure of the Universe as the power spectrum and correlation function of the spatial distribution of dark matter and galaxies. In this paper we show how communication between statistics of the dark matter clustering obtained from numerical simulations and galaxy statistics obtained from large galaxy surveys allows to calculate the power spectrum of the spatial distribution of the galaxies.

Acknowledgments

This work was supported by the project of Ministry of Education and Science of Ukraine (state registration number 0110U001385), research program "Cosmomicrophysics" of the National Academy of Sciences of Ukraine (state registration number 0109U003207) and the SCOPES project No. IZ73Z0128040 of Swiss National Science Foundation.

Appendix A: Fourier modes of dark matter density inhomogeneities

The power spectrum can be derived in more rigorous manner by the series of following mathematical transformations:

$$\delta_{\vec{k}} = \frac{1}{(2\pi)^{\frac{3}{2}} V^{\frac{1}{2}}} \int\limits_V \delta(\vec{r}) e^{i\vec{k}\vec{r}} d^3\vec{r} = \frac{1}{(2\pi)^{\frac{3}{2}} V^{\frac{1}{2}}} \sum_i e^{i\vec{k}\vec{r}_i} \int\limits_{V_i} \frac{\rho(\vec{r}-\vec{r}_i)}{\overline{\rho}} e^{i\vec{k}(\vec{r}-\vec{r}_i)} d^3(\vec{r}-\vec{r}_i)$$

$$= \frac{1}{(2\pi)^{\frac{3}{2}} \overline{\rho} V^{\frac{1}{2}}} \sum_i e^{i\vec{k}\vec{r}_i} m_i \left\{ \frac{1}{m_i} \int\limits_{V_i} \rho(\vec{r}-\vec{r}_i) e^{i\vec{k}(\vec{r}-\vec{r}_i)} d^3(\vec{r}-\vec{r}_i) \right\} = \frac{1}{(2\pi)^{\frac{3}{2}} \overline{\rho} V^{\frac{1}{2}}} \sum_i e^{i\vec{k}\vec{r}_i} m_i y_i(k)$$

$$= \frac{1}{\overline{\rho}} \sum_j n(m_j) m_j \left\{ \frac{1}{(2\pi)^{\frac{3}{2}} V^{\frac{1}{2}} n(m_j)} \sum_{l=1}^{N_j} e^{i\vec{k}\vec{r}_l} y_l(k, m_j) \right\} = \frac{1}{\overline{\rho}} \int\limits_0^\infty m \cdot n(m) \delta_{\vec{k}}(m) \overline{y}(m,k) dm$$

Here, the integration over the whole volume V has been split into integrations over volumes V_i, each occupied by spatially separated halos; the Fourier-transform of i-th density profile we denote as $y_i(k)$, it is normalized by their masses m_i. The halos are binned into the subsets with equal masses m_j, the number of halos is denoted by N_j. Also, it was assumed, that the halos of equal masses have identical density profiles, and correspondingly, their Fourier-transforms, $\overline{y}(m,k)$, are identical too. The $\delta_{\vec{k}}(m)$ is notation of Fourier-amplitude of spatial distribution of halo with masses m. The summation has been changed to the integration.

Appendix B: Fourier modes of galaxy number density inhomogeneities

The Fourier amplitude for relative fluctuations of galaxy concentration takes the following form:

$$\delta_{g|\vec{k}} = \frac{1}{(2\pi)^{\frac{3}{2}} V^{\frac{1}{2}}} \int\limits_V \delta_g(\vec{r}) e^{i\vec{k}\vec{r}} d^3\vec{r}$$

$$= \frac{1}{(2\pi)^{\frac{3}{2}} V^{\frac{1}{2}}} \sum_i e^{i\vec{k}\vec{r}_i} \int\limits_{V_i} \frac{n_g(\vec{r}-\vec{r}_i)}{\overline{n}_g} e^{i\vec{k}(\vec{r}-\vec{r}_i)} d^3(\vec{r}-\vec{r}_i) = \frac{1}{(2\pi)^{\frac{3}{2}} \overline{n}_g V^{\frac{1}{2}}} \sum_i e^{i\vec{k}\vec{r}_i} N_{g|i} \left\{ \frac{1}{N_{g|i}} \int\limits_{V_i} n_g(\vec{r}-\vec{r}_i) e^{i\vec{k}(\vec{r}-\vec{r}_i)} d^3(\vec{r}-\vec{r}_i) \right\}$$

$$= \frac{1}{(2\pi)^{\frac{3}{2}} \overline{n}_g V^{\frac{1}{2}}} \sum_i e^{i\vec{k}\vec{r}_i} N_{g|i} y_{g|i}(k) = \frac{1}{(2\pi)^{\frac{3}{2}} \overline{n}_g V^{\frac{1}{2}}} \sum_m \sum_{j_m} e^{i\vec{k}\vec{r}_{j_m}} N_{g|j_m} y_{g|j_m}(k,m)$$

$$= \frac{1}{\overline{n}_g} \sum_m \overline{y}_g(k,m) \left\{ \frac{1}{(2\pi)^{\frac{3}{2}} V^{\frac{1}{2}}} \sum_{j_m} N_{g|j_m} e^{i\vec{k}\vec{r}_{j_m}} \right\} = \frac{1}{\overline{n}_g} \sum_m \overline{y}_g(k,m) \sum_{N=0}^{\infty} N n(m,N) \left\{ \frac{1}{(2\pi)^{\frac{3}{2}} V^{\frac{1}{2}} n(m,N)} \sum_{l_{mN}} e^{i\vec{k}\vec{r}_{l_{mN}}} \right\}$$

$$= \frac{1}{\overline{n}_g} \sum_m \overline{y}_g(k,m) \sum_{N=0}^{\infty} N n(m) p(N|m) \delta_{\vec{k}}(m,N) = \frac{1}{\overline{n}_g} \sum_m n(m) \delta_{\vec{k}}(m) \overline{y}_g(k,m) \sum_{N=0}^{\infty} N p(N|m)$$

$$= \frac{1}{\overline{n}_g} \int\limits_0^{\infty} \langle N|m\rangle \, n(m) \delta_{\vec{k}}(m) \overline{y}_g(k,m) dm,$$

Here, as in Appendix A, the integration over whole volume V was divided into integrations over the number of volumes V_i, filled by spatially separated halos. The Fourier-images of profiles of concentration of galaxies in halo are normalized by their number $N_{g|i}$; the Fourier-image of i-th profile of galaxy concentration is denoted by $y_{g|i}(k)$. The halo was partitioned into subsets of equal masses m and normalized by means of index j_m.

It was assumed that halo of equal masses have identical profiles of galaxy concentration, so their Fourier-images $\overline{y}_g(m,k)$ are identical; The sets of halos with equal masses m were partitioned into subsets containing the same number N of galaxies and denoted as $n(m,N)$. The halo concentration $n(m,N)$ is represented as a product of concentration of all halos with mass m and conditional probability of event that these halos contain N galaxies each, $n(m,N) = n(m)p(N|m)$. The designation was introduced for Fourier-amplitude of spatial distribution of halos with masses m and containing N galaxies as $\delta_{\vec{k}}(m,N)$. It was assumed, that spatial distribution of halos of mass m and number of galaxies N match the spatial distribution of all halos with masses m, $\delta_{\vec{k}}(m) = \delta_{\vec{k}}(m,N)$. The average number of galaxies in halo of mass m is denoted as $\langle N|m\rangle = \sum\limits_{N=0}^{\infty} N p(N|m)$, also the sum was replaced by intergration.

[1] E. Bertschinger, Astrophys. J. Suppl. **137**, 1 (2001).
[2] S. Edwin, Astroph. J. **634**, 728 (2005).
[3] S.D.M. White, M. Rees, Mon. Not. R. Astron. Soc. **183**, 341 (1978).
[4] A. Benson, Phys. Rep. **495**, 33 (2010).
[5] C. Safranek-Shrader, V. Bromm, M. Milosavljevic, Astrophys. J. **723**, 1568 (2010).
[6] N. Katz, D.H. Weinberg, L. Hernquist, Astrophys. J. Suppl. **105**, 19 (1996).
[7] V. Springel, L. Hernquist, Mon. Not. R. Astron. Soc. **339**, 289 (2003).
[8] G. Kauffmann, S.D.M. White, B. Guiderdoni, Mon. Not. R. Astron. Soc. **264**, 201 (1993).
[9] S. Cole, A. Aragon-Salamanca, C.S. Frenk, J.F. Navarro, S.E. Zepf, Mon. Not. R. Astron. Soc. **271**, 781 (1994).
[10] R.S. Somerville, J.R. Primack, Mon. Not. R. Astron. Soc. **310**, 1087 (1999).
[11] D.J. Croton *et al.*, Mon. Not. R. Astron. Soc. **365**, 11 (2006).
[12] R.G. Bower, A.J. Benson, R. Malbon, J.C. Helly *et al.*, Mon. Not. R. Astron. Soc. **370**, 645 (2006).
[13] X. Yang, H. Mo, F. van den Bosch, Mon. Not. R. Astron. Soc. **339**, 1057 (2003).
[14] X. Yang, H.J. Mo, Y.P. Jing, F.C. van den Bosch, Y. Chu, Mon. Not. R. Astron. Soc. **350**, 1153 (2004).
[15] F.C. van den Bosch, X. Yang, H.J. Mo, S.M. Weinmann, A.V. Macciò et al., Mon. Not. R. Astron. Soc. **376**, 841 (2007).
[16] B. Moster, R. Somerville, C. Maulbetsch, F. van den Bosch et al, Astroph. J. **710**, 903 (2010).
[17] Q. Guo, S. White, C. Li, M. Boylan-Kolchin, Mon. Not. R. Astron. Soc. **404**, 1111 (2010).
[18] J.A. Peacock, R.E. Smith, Mon. Not. R. Astron. Soc. **318**, 1144 (2000).
[19] C.-P. Ma, J.N. Fry, Astrophys. J. **531**, L87 (2000).
[20] U. Seljak, Mon. Not. R. Astron. Soc. **318**, 203 (2000).
[21] A.A. Berlind, D.H. Weinberg, Astrophys. J. **550**, 212 (2002).

[22] A. Cooray, R. Sheth, Physics Reports, **372**, 1 (2002).
[23] H. Gil-Mariń, R. Jimenez, L. Verde, Mon. Not. R. Astron. Soc. **414**, 1207 (2011).
[24] C. Giocoli, M. Bartelmann, R.K. Sheth, M. Cacciato, Mon. Not. R. Astron. Soc. **408**, 300 (2010).
[25] A.J.S. Hamilton, M. Tegmark, Mon. Not. R. Astron. Soc. **330**, 506 (2002).
[26] M. Tegmark, M.R. Blanton, M.A. Strauss, F. Hoyle *et al.*, Astrophys. J. **606**, 702 (2004).
[27] C. Giocoli, G. Tormen, R.K. Sheth, F.C. van den Bosch, Mon. Not. R. Astron. Soc. **404**, 502 (2010).
[28] R.C. Tolman, *Relativity, thermodynamics and cosmology* (Oxford, Clearendon Press, 1969).
[29] Yu. Kulinich, Kinematics and Physics of Celestial Bodies **24**, 121 (2007).
[30] Yu. Kulinich, B. Novosyadlyj, V. Pelykh, J. Phys. Stud. **11**, 473 (2007).
[31] B.S. Novosyadlyi, V.A. Pelykh, Soviet. Astr. (tr: A. Zhurn.) **32**, 231 (1988).
[32] Yu. Kulinich, B. Novosyadlyj, J. Phys. Stud., **7**, 234 (2003).
[33] P.J.E. Peebles, *The large-scale structure of the universe* (Princeton University Press, Princeton, N.J., 1980).
[34] V.R. Eke, S. Cole, C.S. Frenk, Mon. Not. R. Astron. Soc. **282**, 263 (1996).
[35] G.M. Voit, Rev. of Mod. Phys. **77**, 207 (2005).
[36] W. Saslaw, *Gravitational physics of stellar and galactic system* (Cambridge University Press, Cambridge, England, 1987).
[37] M. Vogelsberger, S.D.M. White, Mon. Not. R. Astron. Soc. **413**, 1419 (2011).
[38] M. Kuhlen, N. Weiner, J. Diemand, *et al.*, J. Cosmol. Astropart. Phys. **02**, 030 (2010).
[39] M. Fairbairn, T. Schwetz, J. Cosmol. Astropart. Phys. **01**, 037 (2009).
[40] S.H. Hansen, B. Moore, New Astron. **11**, 333 (2006).
[41] J. Navarro, C. Frenk, S. White, Astroph. J. **490**, 493 (1997).
[42] Y.P. Jing, Astroph. J. **535**, 30 (2000).
[43] J.S. Bullock, T.S. Kolatt, Y. Sigad, R.S. Somerville *et al.*, Mon. Not. R. Astron. Soc. **321**, 559 (2001).
[44] V. Eke, J. Navarro, M. Steinmetz, Astroph. J. **554**, 114 (2001).
[45] A. Duffy, J. Schaye, S. Kay, V. Dalla, Mon. Not. R. Astron. Soc. Letters **390**, L64 (2008).
[46] E. Komatsu, J. Dunkley, M. Nolta, C. Bennett et al, Astroph. J. Suppl., **180**, 330 (2009).
[47] W.H. Press, P. Schechter, Astroph. J. **187**, 425 (1974).
[48] J. Bond, S. Cole, G. Efstathiou, N. Kaiser, Astrophys. J. **379**, 440 (1991).
[49] R.G. Bower, Mon. Not. R. Astron. Soc. **248**, 332 (1991).
[50] C. Lacey, S. Cole, Mon. Not. R. Astron. Soc. **262**, 627 (1993).
[51] R.K. Sheth, G. Tormen, Mon. Not. R. Astron. Soc. **308**, 119 (1999).
[52] R. Sheth, H. Mo, G. Tormen, Mon. Not. R. Astron. Soc. **323**, 1 (2001).
[53] W. Hu, A.V. Kravtsov, Astroph. J. **584**, 702 (2003).
[54] M. Davis, G. Efstathiou, C.S. Frenk, S.D.M. White, Astrophys. J. **292**, 371 (1985).
[55] C. Lacey, S. Cole, Mon. Not. R. Astron. Soc. **271**, 676 (1994).
[56] A. Jenkins, C.S. Frenk, S.D.M. White, J.M. Colberg *et al.*, Mon. Not. R. Astron. Soc. **321**, 372 (2001).
[57] A.F. Neto, L. Gao, P. Bett, S. Cole *et al.*, Mon. Not. R. Astron. Soc. **381**, 1450 (2007).
[58] A. Maccio, A. Dutton, F. van den Bosch, Mon. Not. R. Astron. Soc. **391**, 1940 (2008).
[59] G. Kauffmann, J.M. Colberg, A. Diaferio, S.D.M. White, Mon. Not. R. Astron. Soc. **303**, 188 (1999).
[60] J. Tumlinson, Astrophys. J. **708**, 1398 (2010).
[61] V. Springel, S.D.M. White, G. Tormen, G. Kauffmann, Mon. Not. R. Astron. Soc. **328**, 726 (2001).
[62] P. Bode, J.P. Ostriker, N. Turok, Astrophys. J. **556**, 93 (2001).
[63] L. Gao, S.D.M. White, J. Jenkins, F. Stoehr, V. Springel, Mon. Not. R. Astron. Soc. **355**, 819 (2004).
[64] P.J.E. Peebles, *Principles of Physical Cosmology* (Princeton University Press, Princeton, N.J., 1993).
[65] G. Efstathiou, J.R. Bond, S.D.M. White, Mon. Not. R. Astron. Soc. **258**, 1 (1992).
[66] J. Peacock, S. Dodds, Mon. Not. R. Astron. Soc. **280**, L19 (1996).
[67] R. Smith, J. Peacock, A. Jenkis, S.D. White, C.S. Frenk et al, Mon. Not. R. Astron. Soc. **341**, 1311 (2003).
[68] A.J.S. Hamilton, P. Kumar, E. Lu, A. Matthews, Astroph. J. **374**, L1 (1991).
[69] M. Viel, K. Marković, M. Baldi, J. Weller, 2011, eprint arXiv:1107.4094.
[70] S.H. Hansen, J. Lesgourgues, S. Pastor, J. Silk, Mon. Not. R. Astron. Soc. **333**, 544 (2002).
[71] M. Viel, J. Lesgourgues, M.G. Haehnelt, S. Matarrese, A. Riotto, Phys. Rev. D **71**, id. 063534 (2005)
[72] R. Smith, K. Marković, Phys. Rev. D **84**, id. 063507 (2011).
[73] Q. Guo, S. Cole, V. Eke, C. Frenk, 2012, eprint arXiv:1201.1296
[74] A. Lewis, A. Challinor and A. Lasenby, Astrophys. J. **538**, 473 (2000).
[75] http://camb.info